Estimating rice yield related traits and quantitative trait loci analysis under different nitrogen treatments using a simple tower-based field phenotyping system with modified single-lens reflex cameras.

Citation:

Naito, Hiroki; Ogawa, Satoshi; Valencia, Milton Orlando; Mohri, Hiroki; Urano, Yutaka; Hosoi, Fumiki; Shimizu, Yo; Chavez, Alba Lucia; Ishitani, Manabu; Gomez Selvaraj, Michael; Omasa, Kenji. 2017. Estimating rice yield related traits and quantitative trait loci analysis under different nitrogen treatments using a simple tower-based field phenotyping system with modified single-lens reflex cameras. ISPRS Journal of Photogrammetry and Remote Sensing 125: 50-62.

Publisher's DOI:

https://dx.doi.org/10.1016/j.isprsjprs.2017.01.010

Access through CIAT Research Online:

http://hdl.handle.net/10568/79357

Elsevier Editorial System(tm) for ISPRS Journal of Photogrammetry and Remote Sensing
Manuscript Draft

Manuscript Number: PHOTO-D-16-00280R3

Title: Estimating rice yield related traits and quantitative trait loci analysis under different nitrogen treatments using a simple tower-based field phenotyping system with modified single-lens reflex cameras

Article Type: Original Research Paper

Section/Category: Optical remote sensing

Keywords: Rice breeding; Field based high throughput phenotyping; Remote sensing; Single lens reflex camera; Vegetation index; Yield related traits

Corresponding Author: Professor Kenji Omasa, PhD

Corresponding Author's Institution: The University of Tokyo

First Author: Hiroki Naito, PhD

Order of Authors: Hiroki Naito, PhD; Satoshi Ogawa, PhD; Milton O Valencia, Master; Hiroki Mohri, Bachelor; Yutaka Urano, PhD; Fumiki Hosoi, PhD; Yo Shimizu, PhD; Alba L Chavez, Master; Manabu Ishitani, PhD; Michael G Selvaraj, PhD; Kenji Omasa, PhD

Response to editor and reviewers

Comments from the Editors and Reviewers:

Here is the comments from Dr Weng --

I read this version, but the vast majority of references are from agronomy journals. As a matter of fact, ISPRS J contains quite a few recent works that the authors can compare to, not to speak of RSE.
Best regards,
Qihao

Response:

We added more literature reviews from remote sensing journals. Following articles are cited in this version:

Barmeier, G., Schmidhalter, U., 2016. High-Throughput Phenotyping of Wheat and Barley Plants Grown in Single or Few Rows in Small Plots Using Active and Passive Spectral Proximal Sensing. Sensors 16(11), 1860. (**Page 9; Line 9**)

Behmann, J., Mahlein, A. K., Paulus, S., Kuhimann, H., Oerke, E. C., Plümer, L., 2015. Calibration of hyperspectral close-range pushbroom cameras for plant phenotyping. ISPRS Journal of Photogrammetry and Remote Sensing 106, 172-182. (**Page 10; Line 13**)

Colomina, I., Molina, P., 2014. Unmanned aerial systems for photogrammetry and remote sensing: A review. ISPRS Journal of Photogrammetry and Remote Sensing 92, 79-97. (**Page 9; Line 15**)

He, L., Song, X., Feng, W., Guo, B. B., Zhang, Y. S., Wang, Y. H., Wang, C. Y., Guo, T. C., 2016. Improved remote sensing of leaf nitrogen concentration in winter wheat using multi-angular hyperspectral data. Remote Sensing of Environment 174, 122-133. (**Page 10; Line 11**)

Moharana, S., Dutta, S., 2016. Spatial variability of chlorophyll and nitrogen content of rice from hyperspectral imagery. ISPRS Journal of Photogrammetry and Remote Sensing 122, 17-29. (**Page 10; Line 11**)

Yu, N., Li, L., Schmitz, N., Tian, L. F., Greenberg, J. A., Diers, B. W., 2016. Development of methods to improve soybean yield estimation and predict plant

maturity with an unmanned aerial vehicle based platform. Remote Sensing of Environment 187, 91-101. (**Page 9; Line 13**)

Zarco-Tejada, P. J., González-Dugo, M. V., Fereres, E., 2016. Seasonal stability of chlorophyll fluorescence quantified from airborne hyperspectral imagery as an indicator of net photosynthesis in the context of precision agriculture. Remote Sensing of Environment 179, 89-103. (**Page 10; Line 12**)

-----Original Message-----

From: eesserver@eesmail.elsevier.com [mailto:eesserver@eesmail.elsevier.com]
Sent: Wednesday, December 14, 2016 2:03 PM
To: aomasa@mail.ecc.u-tokyo.ac.jp
Subject: Accept pending requirements

Manuscript No.: PHOTO-D-16-00280R2
Title: Estimating rice yield related traits and quantitative trait loci analysis under different nitrogen treatments using a simple tower-based field phenotyping system with modified single-lens reflex cameras Article Type: Original Research Paper Corresponding Author: Professor Kenji Omasa All Authors: Hiroki Naito, PhD; Satoshi Ogawa, PhD; Milton O Valencia, Master; Hiroki Mohri, Bachelor; Yutaka Urano, PhD; Fumiki Hosoi, PhD; Yo Shimizu, PhD; Alba L Chavez, Master; Manabu Ishitani, PhD; Michael G Selvaraj, PhD; Kenji Omasa, PhD Submit Date: Jun 21, 2016

Dear Professor Omasa,

Thank you for submitting the above-mentioned article to ISPRS Journal of Photogrammetry and Remote Sensing.

We are pleased to inform you that at this point, the scientific content requires no further revision and we are prepared to officially accept your article.

We have been able to use your submitted paper for the review process and now that the paper is going to go into production, there are a couple of small things that need to be done to ensure smooth processing of your paper through the production process. Please check the "file inventory" to ensure that all of the items listed below are included in your manuscript.

1) Manuscript Source Files:
We cannot accommodate PDF manuscript files for production purposes. Refer to Guide for Authors for additional information: http://www.elsevier.com/journals/isprs-journal of-photogrammetry-and-remote-sensing/0924-2716/guide-for-authors

2) Figure Source Files:

Please make sure that artwork files are in an acceptable format (TIFF, EPS or MS Office files) and with the correct resolution. You may include figure files embedded within the manuscript file, as long as they are of sufficient resolution for Production.
http://www.elsevier.com/artworkinstructions

3) Graphical Abstract (optional)
Graphical Abstracts should summarize the contents of the article in a concise, pictorial form designed to capture the attention of a wide readership online. Authors must provide images that clearly represent the work described in the article. Graphical abstracts should be submitted as a separate file in the online submission system. Image size: Please provide an image with a minimum of 531 × 1328 pixels (h × w) or proportionally more. The image should be readable at a size of 5 × 13 cm using a regular screen resolution of 96 dpi. Preferred file types: TIFF, EPS, PDF or MS Office files. See http://www.elsevier.com/graphicalabstracts for examples.

When submitting your final files, be sure to include a separate document uploaded as "Response to Reviewers" that confirms you have provided all of the requested items that were previously not present (for example, "highlights have now been uploaded").

Please submit your files online by logging onto the Elsevier Editorial System for ISPRS Journal of Photogrammetry and Remote Sensing as an Author:
http://ees.elsevier.com/photo
Your username is: aomasa@mail.ecc.u-tokyo.ac.jp If you need to retrieve password details, please go to: http://ees.elsevier.com/photo/automail_query.asp

PLEASE NOTE: ISPRS Journal of Photogrammetry and Remote Sensing would like to enrich its relevant online articles by displaying 3D models that allow the reader to interactively explore the underlying research data. Hence, if applicable, we would like to invite you to upload with your manuscript 3D models (in OBJ, PLY or U3D data format) as supplementary material to our online submission system. Elsevier will generate the interactive viewer for your datasets and include it with the online article on ScienceDirect. More information can be found at: http://www.elsevier.com/about/content-innovation/obj-ply-models and http://www.elsevier.com/about/content-innovation/u3d-models

ISPRS Journal of Photogrammetry and Remote Sensing features the Interactive Plot Viewer,

see: http://www.elsevier.com/interactiveplots. Interactive Plots provide easy access to the data behind plots. To include one with your article, please prepare a .csv file with your plot data and test it online at http://authortools.elsevier.com/interactiveplots/verification before submission as supplementary material.

PLEASE NOTE: The journal would like to enrich online articles by visualising and providing geographical details described in ISPRS Journal of Photogrammetry and Remote Sensing articles. For this purpose, corresponding KML (GoogleMaps) files can be uploaded in our online submission system. Submitted KML files will be published with your online article on ScienceDirect. Elsevier will generate maps from the KML files and include them in the online article.

ISPRS Journal of Photogrammetry and Remote Sensing features the Interactive Map Viewer, http://www.elsevier.com/googlemaps. Interactive Maps visualize geospatial data provided by the author in a GoogleMap. To include one with your article, please submit a .kml or .kmz file and test it online at http://elsevier-apps.sciverse.com/GoogleMaps/verification before uploading it with your submission.

We once again thank you for your contribution to ISPRS Journal of Photogrammetry and Remote Sensing and look forward to publishing your work.

Yours sincerely,

Xin Miao
Associate Editor
ISPRS Journal of Photogrammetry and Remote Sensing

Comments from the Editors and Reviewers (if available):

Here is the comments from Dr Weng --

I read this version, but the vast majority of references are from agronomy journals. As a matter of fact, ISPRS J contains quite a few recent works that the authors can compare to, not to speak of RSE.
Best regards,

Qihao

Please revise accordingly.

Title

Estimating rice yield related traits and quantitative trait loci analysis under different nitrogen treatments using a simple tower-based field phenotyping system with modified single-lens reflex cameras

Author names and affiliations

Hiroki Naito[a], Satoshi Ogawa[a,b] Milton Orlando Valencia[b], Hiroki Mohri[a], Yutaka Urano[a], Fumiki Hosoi[a], Yo Shimizu[a], Alba Lucia Chavez[b], Manabu Ishitani[b], Michael Gomez Selvaraj[b] * and Kenji Omasa[a]*

[a] Graduate School of Agricultural and Life Sciences, The University of Tokyo, Yayoi 1-1-1, Bunkyo-ku, Tokyo, Japan, 113-8657

[b] International Center for Tropical Agriculture (CIAT), A.A. 6713, Cali, Colombia

Email address list:

Hiroki Naito: hiroki.naito@outlook.com

Satoshi Ogawa: gawao59@gmail.com

Milton Orlando Valencia: m.o.valencia@cgiar.org

Hiroki Mohri: hirokimohri29@gmail.com

Yutaka Urano: rich@lime.plala.or.jp

Fumiki Hosoi: ahosoi@mail.ecc.u-tokyo.ac.jp

Yo Shimizu: ayosh@mail.ecc.u-tokyo.ac.jp

Alba Lucia Chavez: a.l.chavez@cgiar.org

Manabu Ishitani: m.ishitani@cgiar.org

Michael Gomez Selvaraj: m.selvaraj@cgiar.org

Kenji Omasa: aomasa@mail.ecc.u-tokyo.ac.jp

*** Co-corresponding authors:**

Dr. Kenji Omasa

Graduate School of Agricultural and Life Sciences

The University of Tokyo, Yayoi 1-1-1, Bunkyo-ku

Tokyo, Japan, 113-8657

e.mail : aomasa@mail.ecc.u-tokyo.ac.jp

Tel : +81-3-5841-5340

Dr. Michael Gomez Selvaraj

International Center for Tropical Agriculture (CIAT),

A.A. 6713, Cali, Colombia

e.mail: m.selvaraj@cgiar.org

Tel : +57-2-4450000 Ext: 3353

Abstract:

Application of field based high-throughput phenotyping (FB-HTP) methods for monitoring plant performance in real field conditions has a high potential to accelerate the breeding process. In this paper, we discuss the use of a simple tower based remote sensing platform using modified single-lens reflex cameras for phenotyping yield traits in rice under different nitrogen (N) treatments over three years. This tower based phenotyping platform has the advantages of simplicity, ease and stability in terms of introduction, maintenance and continual operation under field conditions. Out of six phenological stages of rice analyzed, the flowering stage was the most useful in the estimation of yield performance under field conditions. We found a high correlation between several vegetation indices (simple ratio (SR), normalized difference vegetation index (NDVI), transformed vegetation index (TVI), corrected transformed vegetation index (CTVI), soil-adjusted vegetation index (SAVI) and modified soil-adjusted vegetation index (MSAVI)) and multiple yield traits (panicle number, grain weight and shoot biomass) across a three trials. Among all of the indices studied, SR exhibited the best performance in regards to the estimation of grain weight (R^2 = 0.80). Under our tower-based field phenotyping system (TBFPS), we identified quantitative trait loci (QTL) for yield related traits using a mapping population of chromosome segment substitution lines (CSSLs) and a single nucleotide polymorphism data set. Our findings suggest the TBFPS can be useful for the estimation of yield performance during early crop development. This can be a major opportunity for rice breeders whom desire high throughput phenotypic selection for yield performance traits.

Key words:

Breeding, Field based high throughput phenotyping, Remote sensing, Rice, Single lens reflex camera, Vegetation index, Yield related traits

Abbreviations

AlaAT: Alanine amino transferase

ANOVA: Analysis of variance

BRDF: Bidirectional reflectance distribution function

CC: Canopy cover index

CCD: Charge coupled device

CIAT: International Center for Tropical Agriculture

CRG: Curinga

CSSLs: Chromosome segment substitution lines

CTVI: Corrected transformed vegetation index

DAT: Days after transplanting

DG: Dough grain stage

DN: Digital number

DVI: Difference vegetation index

EV: Early vegetative phase

F174: Fedearroz 174

FBP: Field based phenotyping

FB-HTP: Field based - High throughput phenotyping

FL: Flowering stage

FM: Fedearroz Mokari

FP: Farmer's practice

GCP: Ground control point

GS: Grain sterility percentage

GW: Grain weight

HTP: High throughput phenotyping

IR64: IR-64

LAI: Leaf area index

LV: Late vegetative phase

LVA: Late vegetative phase -A

LVB: Late vegetative phase -B

MKG: Milk grain stage

MSAVI: Modified soil-adjusted vegetation index

MTG: Mature grain stage

N: Nitrogen

N4: NERICA 4

NDVI: Normalized difference vegetation index

NIR: Near infrared

PH: Plant height

PI: Panicle initiation

PL: Panicle length

PN: Panicle number

PVI: Perpendicular vegetation index

QTLs: quantitative trait locus

R^2: coefficient of determination

RGB: Red, green and blue

RPG: *O. rufipogon*

SAVI: Soil-adjusted vegetation index

SB: Shoot biomass

SLR: Single-lens reflex

SPAD: Soil and plant analyzer development

SR: Simple ratio

T: Transgenic line

TBFPS: Tower-based field phenotyping system

TSAVI: Transformed soil-adjusted vegetation index

TVI: Transformed vegetation index

U. Tokyo: The University of Tokyo

VIs: Vegetation indices

WDVI: Weighted difference vegetation index

WT: Wild type

Introduction

Achieving maximum grain yield with fewer input costs is the ultimate goal of intensive rice production. A key step in this process lies in identifying rice varieties that enable farmers to produce higher yield with minimum use of water and fertilizer. The rapid development of such rice varieties needs an advanced breeding system to surpass the traditional approaches. To accelerate the breeding of novel agricultural traits to produce environmentally adapted varieties with which require fewer input costs, new technologies which bridge the gap between genotype and phenotype are essential for plant researchers (Furbank, 2009; Fiorani and Schurr, 2013; Pieruschka and Lawson, 2015). Now high throughput phenotyping is one of the key technological solutions being explored to fill this gap.

While efforts are being taken to achieve this goal, drawbacks related to the traditional phenotypic methodologies makes this process very slow. Traditional phenotyping methodologies are often time-consuming and labor intensive because of the abundance of manual operations. Since additionally, these methods are often destructive, which makes it impossible to do sequential measurements on the same plant. In order to speed up the varietal development process the development of a high-throughput phenotyping (HTP) platform that allows fully automated crop image acquisition and advanced image processing technology is necessary (Li et al., 2014). Plant analysis via image based systems has been well studied since the 1980s (Omasa, 1990; Omasa et al., 2002), with recent works focused on a broad range of topics within agriculture.

It is suggested that high throughput phenotyping is key to the data mining of the huge sample sets present under field conditions (Araus and Cairns, 2014). Phenotypic

traits are important to archive in order to clarify the black box interactions between the genotype and the environment. This can be accomplished by considering their interaction (George et al., 2014) or through linking the phenotypic data with different -omics data like genomes, transcriptomes, proteomes, metabolomes and metagenomes in field trials (Alexandersson et al., 2014). Thus, there is a need for simple and robust FB-HTP system for estimating phenotypic traits at the field level. Recently, there is a boom of constructing FB-HTP systems worldwide. Some studies propose several types of unique FB-HTP systems with land vehicle platforms (Svensgaard et al., 2014; White and Conley, 2013; Andrade-Sanchez et al., 2014; Barmeier and Schmidhalter, 2016), aerial platforms like blimps, helicopters, and fixed wing planes (Chapman et al., 2014; Liebisch et al., 2015; Zamann-Allah et al., 2015; Gonzalez-Dugo et al., 2015). In recent year, the use of multicopter has been increasing in field phenotyping studies (Sankaran et al., 2015; Haghighattalab et al., 2016; Inostroza et al., 2016; Tattaris et al., 2016; Yu et al., 2016). The history and applications of unmanned aerial system in the field of remote sensing are well reviewed by Colomina and Molina (2014). However, many of these systems come with considerable costs and often require substantial skill to operate. In this paper, we will describe an alternative low-cost, Tower-based field phenotyping system (TBFPS). This system includes low cost RGB and NIR cameras mounted on stable, yet movable, low maintenance towers. Tower based phenotyping platforms have the additional advantages of unmanned continual operation and repeatability (Deery et al., 2014).

To estimate rice yield related traits from towers, the conventional remote sensing approach using vegetation indices (VIs) is an efficient method. VIs have a long history within cereal crops (Jones and Vaughan, 2010) and have been used within rice to

estimate phenotypic traits such as rice yield (Mosleh et al., 2015). In the area of field based phenotyping (FBP), VIs are considered powerful tools in the estimation of important growth traits like chlorophyll concentration, nitrogen (N), leaf area index (LAI), leaf number, plant biomass, and yield (White et al., 2012). In regards to rice research, VIs and near infrared (NIR) imaging approaches have been widely applied to record crop phenology (Sakamoto et al., 2011), estimate LAI (Shibayama et al., 2011), leaf greenness (Shibayama et al., 2012), N uptake (Shibayama et al., 2009) and yield (Harrell et al., 2011; Tubaña et al., 2011; Mosleh et al., 2015). RGB derived parameters without NIR are also available for estimating chlorophyll content and leaf N concentration of rice (Wang et al., 2014). Moreover, hyperspectral imagery is used for crop phenotyping like estimating nitrogen content (Moharana and Dutta, 2016; He et al., 2016), chlorophyll fluorescence (Zalco-Tejada et al., 2016), or constructing hyperspectral 3D plant models (Behmann et al., 2015) in recent years.

Quantitative trait loci (QTL) analysis has become a powerful tool for identifying the genetic factors influencing quantitative traits like yield and other related traits. In recent years, QTL mapping studies have used rapid phenotyping methods like VIs together with conventional and manual phenotyping approaches. Under field conditions, QTLs of several crops (wheat (Pinto et al., 2010; Edae et al., 2014; Graziani et al., 2014; Li et al., 2014; Li et al., 2015; Gao et al., 2015; Kumar et al., 2016), barley (Obsa et al., 2016), corn (Lu et al., 2012; Trachsel et al., 2016), potato (Khan et al., 2015), cotton (Pauli et al., 2016), and forage grass (Merewitz, et al., 2012; Merewitz et al., 2014)) were successfully detected through the use of VIs. As for rice, Henry et al. (2015) evaluated QTL effects of NILs derived from IR64 rice under drought conditions by using the Normalized Difference Vegetation Index (NDVI). In the previous studies,

VIs of plots were obtained by hand-held spectroradiometers like GreenSeeker (Tribmle Navigation Ltd., California, USA) or FieldScout series (Spectrum Technologies, Inc., Illinois, USA). In terms of the throughput, image-based remote sensing technologies can cover a large number of plots in a short time. Trapp et al (2016) identified dry bean's QTLs for image-based NDVI obtained from a multicopter. However, QTL analysis using VIs have not been studied in rice.

In this paper, we discuss the use of a simple TBFPS for estimating yield related traits in rice. The main objective of the present study is (1) to develop a TBFPS to estimate yield related traits in rice (2) to confirm the specific phenological stages at which the traits are highly correlated with spectral VIs to enhance early estimation efficiency and (3) to determine whether our FBP platform improves our ability to identify yield related QTLs using chromosome segment substitution lines (CSSLs).

Materials and methods

2.1. Plant materials and characteristics

Table 1 shows the genotypes and homozygous transgenic lines of rice used in this study. In the 2012 experiment, six genotypes of rice and six homozygous NERICA4 transgenic events (T1 to T6) carrying the pOsAnt1/AlaAT construct from Arcadia Biosciences at Brawley, California, USA were used. In the 2013 experiment, five genotypes of rice and three selected CSSLs (Ogawa et al., 2014a) derived from a cross between 'Curinga' and *Oryza rufipogon* (IRGC 105491) were used. While in the 2014 experiment, 48 CSSLs and their parents were used.

Table 1. Genotypes and check cultivars used in this study.

Variety	Origin	Group	Ecosystem	Experiment
NERICA4	Africa	*japonica x O. glaberrima*	Lowland	2012 / 2013
NERICA4: T1, T2, T3,T4, T5,T6	Arcardia Inc.,	NERICA4 + AlaAT gene	Lowland	2012
Curinga	Brazil	*Tropical japonica*	Upland	2012 / 2013 / 2014
IR64	Philippines	*indica*	Lowland	2012
Fedearroz 174	Colombia	*indica*	Lowland	2012 / 2013
Fedearroz Mokari	Colombia	*indica*	Lowland	2012
O. rufipogon (IRGC 105491)	South Asia	*Wild speacies*	-	2012 / 2013 / 2014
CT21375	CIAT	*indica*	Lowland	2013
CSSLs 106, 115 and 120	CIAT	Curinga *x O. rufipogon*	-	2013
CSSLs from 101 to 148	CIAT	Curinga *x O. rufipogon*	-	2014

1

2.2. Experimental plot design of N omission field

Paddy field experiments were carried out at the confined N omission field facility, International Center for Tropical Agriculture (CIAT), Palmira, Colombia (3°30'N, 76°21'W).The site receives 1000 mm annual rainfall, is 965 meters above sea level, and has an annual average temperature of 26 °C. Field experiments were conducted over three years (Fig. 1); one during a dry season (August to December, 2012), one during a rainy season (January to June, 2013), and again during a dry season (August to December, 2014). Residual N was depleted from the field trial site prior to planting by cultivating maize over two consecutive seasons with no fertilizer application (Ogawa et al., 2014b). The 2012 and 2013 experiments focused on the development of the tower based FBP platform and the confirmation of the best growth stages to estimate phenotypic traits. The 2014 experiment focused on the validation to the FBP platform methodology using CSSLs.

The experiments were in a split plot design with three N treatments and three replicates for each treatment. There was a difference in plot size between years. In 2012 and 2014, plot size was roughly 0.9 m^2, while in 2013 plot size was 1.8 m^2. Two different treatment regimens were applied. In 2012 and 2013, three N treatments were applied which consisted of 0kg, 90 kg or 180 kg of N. While in 2014 the 90 kg was omitted. The amount of 180 kg N ha^{-1} is Farmer's practice (FP) in Colombia (Berrio et al., 2002), The 0 kg N treatment (Native) consisted of 0 kg ha^{-1} N application. The 90 kg and the 180 kg N treatments were split between three equal applications; 2 days after transplanting (DAT), 10 DAT, and 30 DAT. The other nutrients (KH_2PO_4; 70 kg, KCl; 60 kg, $ZnSO_4$: 25 kg, $FeSO_4$: 80 kg, B: 0.4 kg and 60 kg of micronutrient ha^{-1}) were applied at the same dose across all treatments per the standard commercial rate of

Colombia at two DAT. Integrated agronomic practices were utilized throughout the duration of the experiments to control pests and weeds. Seeds were sowed in trays with soil and a single seedling was transplanted per hill at 21 days after sowing at a spacing of 20 cm between hills and 25 cm between rows. We also adopted staggered transplanting to synchronize the flowering time between the genotypes. To avoid nitrogen loss via ammonia volatilization and denitrification every N application was conducted over dry soil followed by mild irrigation.

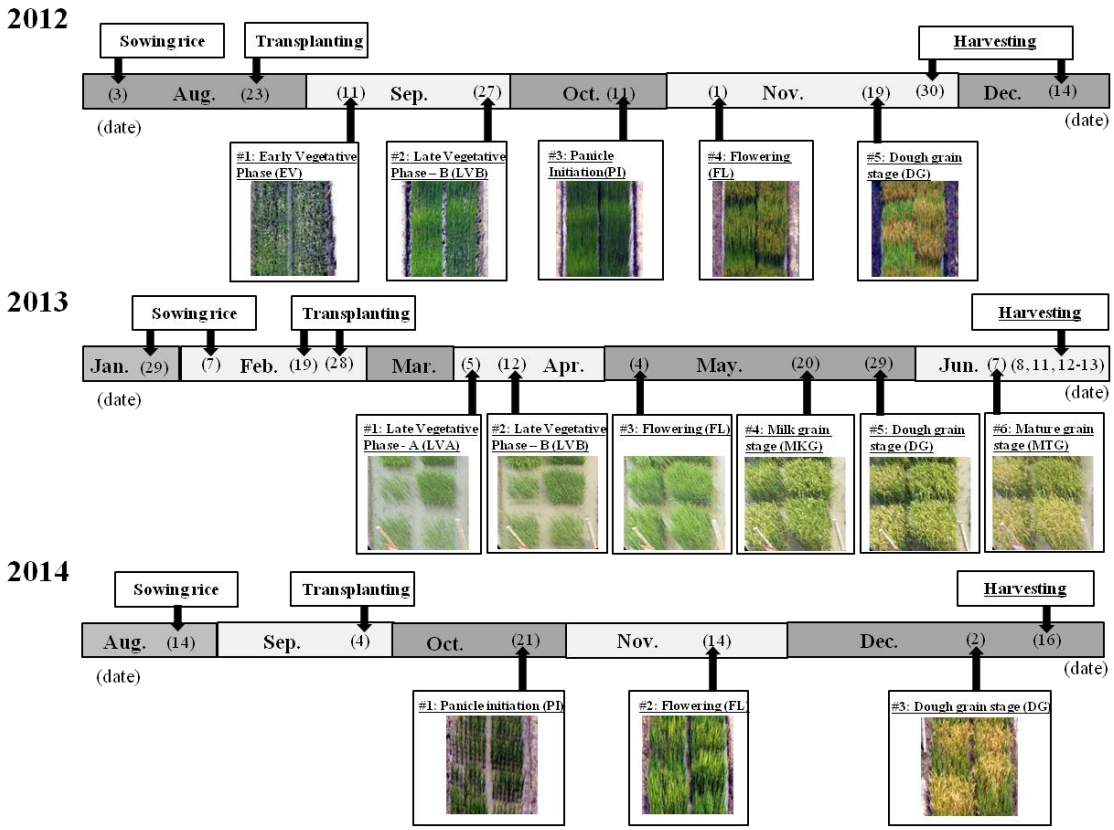

Fig. 1. Schedules of the three experiments in this study. Yield related traits were collected at harvest. Vegetation indices were derived from image data taken at each growth phase and compared to the yield related traits.

2.3. Tower based field phenotyping system

The phenotyping platform at CIAT consists of three towers installed around the N rice field. In this study, only two towers were used for image analysis (Fig. 2 (a)). The height of the towers are eight meters. The towers have been fitted with a multispectral single-lens reflex camera system for image acquisition.

Our multispectral image system composed of two cameras; a single-lens reflex (SLR) camera D300s (Nikon Imaging Japan Inc., Tokyo, Japan) and a modified SLR camera D80 (Nikon Imaging Japan Inc., Tokyo, Japan). The Nikon D300s has three visible bands: red, green and blue. The Nikon D80 camera has single NIR band; it was modified with an inbuilt high pass filter IR-85 (HOYA Corp., Tokyo, Japan; transition wavelength > 850nm) on the CCD sensor to capture in NIR wavelength regions. Viewing angles are shown in Fig. 2 (b). Images from eight angles were captured from the side view and were processed and used to retrieve VIs. Each image was taken at around noon in order to keep the solar zenith angle minimum and avoid any shadow effects in the observed images. Imaging of plot areas were affected by the distance from towers, therefore multiple replication plots of the same genotypes (e.g. near plot, middle plot and far plot from towers) were averaged to minimize the influence.

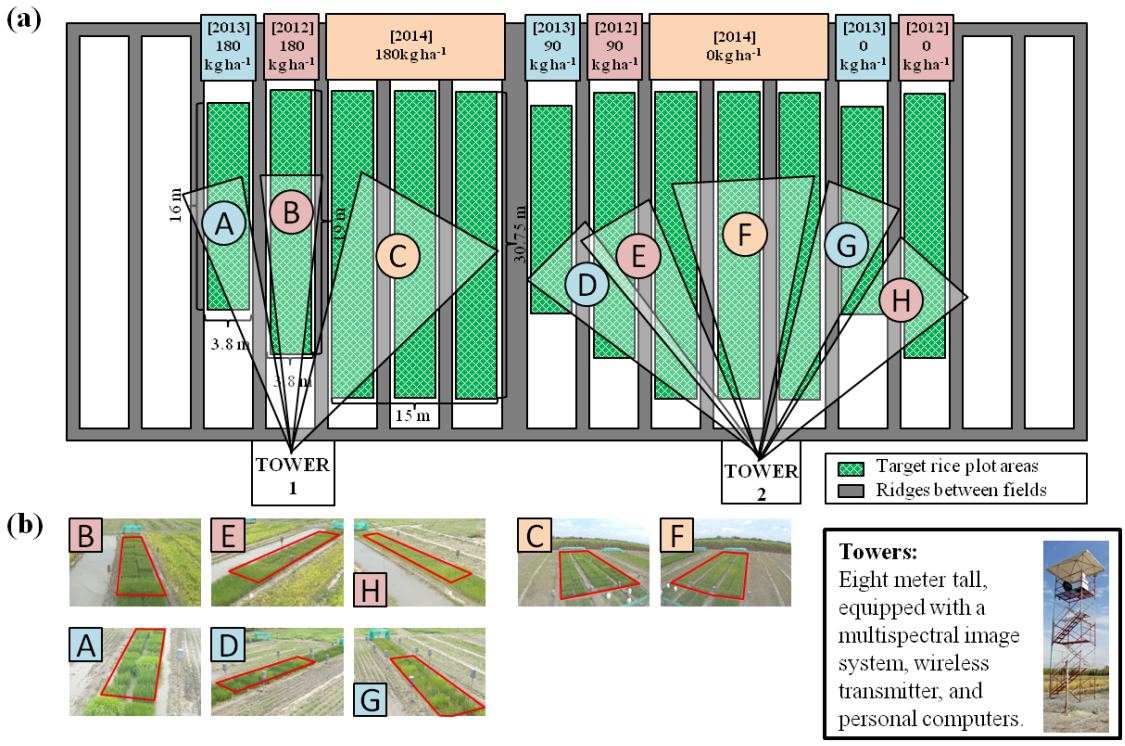

Fig. 2. Experimental map and viewing angles of this study (Year 2012: angle B, E, and H; Year 2013: angle A, D, and G; Year 2014: angle C and F). (a) Each square in the field represents target areas of this study. Measurements of three N treatment fields (0 kg 60 kg ha^{-1}, and 180 kg ha^{-1}) were held from two measurement towers (Tower 1 and Tower 2) by using two type of cameras (NIR camera and visible camera). (b) Examples of obtained visible images by this system. The inside areas of red lines represent target rice areas of this study. All example images were taken at flowering time.

2.4. Image processing for calculating VIs

Images obtained from the multispectral imaging system were processed in the following steps (Fig. 3).

1) *Image registration*:

Visible images obtained by the RGB camera are split to three bands (red, green, and blue). Adding NIR images to the red, green and blue images, the four images were transformed into the same coordinate system by affine transformation in the image registration tool of general remote sensing software ENVI (Exelis VIS, Inc., Boulder, USA). The transformation was based on the ground control points (GCPs) specified at the four vertexes of the rectangular field area between images.

2) *Conversion to reflectance*:

The original images are recorded as 8-bit digital numbers (DN). In this procedure, the DN values were converted to reflectance in order to normalize brightness variation. Conversion was performed by referencing to gray color box's upper surfaces installed in the field as reflection references. The reflectance $R_{x,y,\lambda}$ of the target pixel at coordinates (x, y) in the wavelength λ image was proportionally defined as:

$$R_{x,y,\lambda} = \frac{DN_{x,y,\lambda}}{DN_{ref,\lambda}} R_{ref,\lambda} \quad (1)$$

where $DN_{x,y,\lambda}$, $DN_{ref,\lambda}$, and $R_{ref,\lambda}$ represents the digital number of the target pixel, the digital number of the gray box reference, and the reflectance value of the gray box reference, respectively. $DN_{ref,\lambda}$ were obtained by averaging pixel's DN within the gray box area in the images. Prior to the experiment, reflectance of the gray color boxes $R_{ref,\lambda}$ was measured using a spectrometer V-570 (JASCO Corp., Tokyo, Japan) equipped with an integrating sphere ISN-470 (JASCO Corp., Tokyo,

Japan) under laboratory conditions. The measurement wavelength range was set from 400 nm to 1200 nm with a spectral resolution of 1 nm. The reflectance values at the peak wavelengths of each multispectral band were used for the calculation (1). Because the reflectance of the gray boxes was almost constant in each camera spectral band, we did not integrate the spectrum to match the wavelength resolution between the cameras and the spectrometer by using camera's spectral response functions.

3) *Geometric transformation*:

As images were obtained from the towers and thus were not from nadir, the rectangular shape of the rice fields were distorted within the images to a trapezoid. By skew correction, distorted field images are geometrically transformed to rectangle shape in order to make plot area separation easier on the images. The affine transformation and nearest neighbor algorithm were used as geometrical transformation methods during image registration within ENVI.

4) *Specification of plot areas*:

After skew correction, we specified the assessment area of each plot manually. The areas were selected to include only the upper side of the crop canopy. At the upper planes of the canopy, reflectance characteristics comparatively change based on the period of rice growth (ex. leaves are dominant on vegetative phase or panicles are dominant after flowering time). The plot areas were selected by using the region of interest tool of ENVI. Reflectance of each plot area was derived by averaging all pixels within the plot area. These reflectance values were used for the variables in the VI's formulas described below.

5) *Calculation of VIs and CC*:

We calculated VIs and canopy cover index (CC) of each plot area separately. The VIs and CC were automatically calculated by using our developed IDL program (Exelis VIS, Inc., Boulder, USA).

In total 11 VIs were used in this study (Table 2). We selected general VIs from previous reports for validation (Silleos et al., 2006; Jones and Vaughan, 2010). In 2014, we selected six VIs (SR, NDVI, CTVI, SAVI, DVI, MSAVI) based on the results of the 2012 and 2013 experiments. In regards to the VIs, both the Transformed Vegetation Index (TVI) and Corrected Transformed Vegetation Index (CTVI) are modifications of NDVI. The Soil-Adjusted Vegetation Index (SAVI) is intended to minimize the background soil effect on the vegetation signal by incorporating a constant soil adjustment factor L into the denominator of the NDVI formula. In order to reduce the soil effect, the Perpendicular Vegetation Index (PVI), Transformed Soil-Adjusted Vegetation Index (TSAVI), and Weighted Difference Vegetation Index (WDVI) use 'soil line' parameters in their equations. In order to acquire the soil line parameters from the images, we sampled various bare soil pixels around the rice plot. From the sampled pixels, we drew a linear regression line defined as a soil line in red and NIR reflectance space. Then we defined the slope and intercept parameters of the soil line as the objective soil line parameters.

CC is one of the most important parameters in every imaging platform for crop phenotyping (Table 2). It is well known that CC is a good indicator of plant early growth development, because CC is positively correlated to tiller number, LAI, and biomass (Li et al., 2010). Here CC is defined as the proportion of pixels covered by canopy against the total of the whole area's pixels. CC is often derived from the red and green digital numbers in RGB cameras (Li et al., 2010; Wang et al., 2013),

whereas our imaging system adopted NDVI as the indicator of foliage pixels. The threshold of NDVI was determined by the iterated discriminant analysis method (Otsu, 1975). CC is normally derived from images viewed from nadir, while we investigated the usability of CC obtained from towers, which provided non-nadir images, in this study.

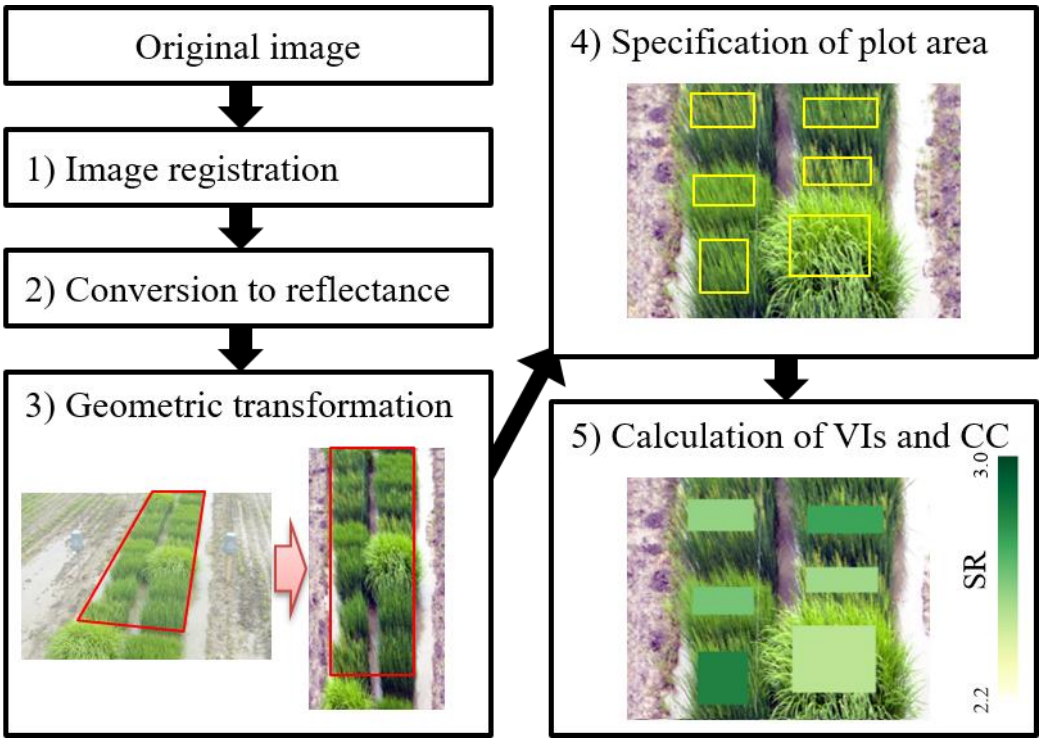

Fig. 3. Flowchart of image processing for calculating VIs and CC. 3) Geometric transformation: Distorted original images (Left) were geometrically transformed to images that plot area is rectangle shape (Right). 4) Specification of plot areas: rectangle areas were target plot areas that were designated manually from images. 5) VIs and CC were automatically calculated on specified plot areas by created IDL programs. An example of the spatial variation of Simple Ratio (SR) is shown in the figure. All example images in this figure were taken at the 180 kg ha^{-1} nitrogen field of flowering time in the 2013 experiment.

Table 2. VIs formula used in this study. This study compared total 11 VIs. ρ_{NIR}, $\rho_{Red,}$ and ρ_{Green} indicate spectral reflectance in the NIR, Red and Green bands, respectively.

Vegetation Index	Formula	Reference
Simple ratio	$SR = \frac{\rho_{NIR}}{\rho_{Red}}$	Birth and McVey (1968)
Normalized Difference Vegetation Index	$NDVI = \frac{\rho_{NIR} - \rho_{Red}}{\rho_{NIR} + \rho_{Red}}$	Rouse et al. (1974)
Green Normalized Difference Vegetation Index	$GNDVI = \frac{\rho_{NIR} - \rho_{Green}}{\rho_{NIR} + \rho_{Green}}$	Gitelson et al. (1996)
Transformed Vegetation Index	$TVI = \sqrt{\frac{\rho_{NIR} - \rho_{Red}}{\rho_{NIR} + \rho_{Red}}} + 0.5$	Derring et al. (1975)
Corrected Transformed Vegetation Index	$CTVI = \frac{NDVI + 0.5}{ABS(NDVI + 0.5)} \times \sqrt{ABS(NDVI + 0.5)}$	Perry and Lautenschlager (1984)
Soil-Adjusted Vegetation Index	$SAVI = \frac{\rho_{NIR} - \rho_{Red}}{\rho_{NIR} + \rho_{Red} + L}(1 + L)$	Huete (1988)
Difference Vegetation Index	$DVI = \rho_{NIR} - \rho_{Red}$	Tucker (1979)
Perpendicular Vegetation Index	$PVI = \frac{(b\rho_{NIR} - \rho_{Red}) + a}{\sqrt{b^2 + 1}}$	Perry and Lautenschlager (1984)
Transformed Soil-Adjusted Vegetaion Index	$TSAVI = \frac{a(\rho_{NIR} - a\rho_{Red} - b)}{\rho_{Red} + a\rho_{NIR} - ab + 0.08(1 + a^2)}$	Baret and Guyot (1991)
Modified Soil-Adjusted Vegetation Index	$MSAVI = \frac{2\rho_{NIR} + 1 - \sqrt{(2\rho_{NIR} + 1)^2 - 8(\rho_{NIR} - \rho_{Red})}}{2}$	Qi et al. (1994)
Weighted Difference Vegetation Index	$WDVI = \rho_{NIR} - \gamma\rho_{Red}$	Richardson and Wiegand (1977); Clevers (1988)

a, γ = slope of soil line, b = intercept of soil line, L = soil effect coefficient (0.25 in this study)

2.5. Trait measurement and regression analysis

In this experiment, six yield related traits were measured at harvest: panicle number (PN), grain weight (GW), shoot biomass (SB), grain sterility percentage (GS), plant height (PH), and panicle length (PL). Significant variations in analysis of variance (ANOVA) were observed in agronomic traits between the genotype, N treatment, and their interactions (Table 3). To demonstrate the feasibility of VIs to estimate the phenotype, regression analyses were performed. Simple linear regression was used as a statistical prediction model between the six yield related traits and 11 VIs. The VIs were derived from the images captured at key phenological growth stages of rice (Fig. 1). The points of time were the followings: early vegetative phase (EV), late vegetative phase (LV), panicle initiation (PI), flowering stage (FL), and dough grain stage (DG) in the 2012 experiment; late vegetative phase -A (LVA), late vegetative phase –B (LVB), flowering stage (FL), milk grain stage (MKG), dough grain stage (DG), mature grain stage (MTG) in the 2013 experiment; panicle initiation (PI), flowering stage (FL), and dough grain stage (DG) in the 2014 experiment. The analyses included all N treatments to make the regression model. Replicates of the same genotypes were averaged before the regression analysis. Sample sizes were 36 (12 genotypes × three treatments) in the 2012 experiment and 24 (eight genotypes × three treatments) in the 2013 experiment. The acquired coefficients of determination (R^2) was evaluated and discussed.

As a first step, the spatial and temporal (growth stage) variations within each of the VIs were examined. The spatial variation in yield related traits at harvest were also examined. Using the Simple Ratio (SR) as an example, we confirmed which factors or genotypic variations caused the correlation between VIs and yield related traits in the following results. Second, we determined the promising combinations of traits and VIs

for the yield related traits estimation. We did this by comparing the R^2 results between the six yield related traits and the all VIs obtained at flowering stage in the 2012 and 2013 experiment. The flowering stage was selected based on the R^2 values which revealed the best performance occurred during this stage. This is supported by previous work which suggested that peak greenness often coincides with flowering and thus is used in the event of forecasting rice yield (Mosleh et al., 2015). Third, to confirm the effective image capture periods, we examined the time series of R^2 between grain weight and VIs during rice lifecycle in the both 2012 and 2013 experiments. We focused only on grain weight, because it is one of the most important traits related to agronomic N use efficiency. Forth, we determined the best VI and imaging time for grain weight estimation by examining R^2 values of reproductive phases in detail. Finally, under N deficit conditions, we estimated the response of grain weight by using the best VI and imaging time. Specifically, multiple comparison of grain weight was performed between different N treatments on each genotype. The different N treatments and genotypes were separately handled in this analysis. Multiple comparison of the VI was also performed similarly. Sample sizes of each comparison were nine on the VI and 21 on grain weight at the maximum.

Table 3. **S**ignificant difference (ANOVA) of selected yield related traits under three different N applications over two seasons. In the table, *Genotype* and *Treatments* indicates main effects and *G x T* indicates their interactions in the ANOVA tests.

		PN	GW	SB	GS	PH	PL
2012	*Genotype*	**	**	**	**	**	**
	Treatment	**	**	**	**	**	**
	G x T	*	**	**	**	**	**
2013	*Genotype*	**	**	**	**	**	**
	Treatment	**	**	**	**	**	**
	G x T	NS	**	**	**	**	*
2014	*Genotype*	**	**	**	**	**	**
	Treatment	**	**	**	NS	**	**
	G x T	**	**	**	**	**	**

PN: Panicle number; GW: Grain weight; SB: Shoot biomass; GS: Grain sterility percentage; PH: Plant height; PL: Panicle length

*, ** indicate significance at 0.05 and 0.01 levels, respectively. NS indicates no significance

2.6 Identification of QTLs using image-based field phenotyping system

In the 2014 experiment, regression analyses between yield related traits and VIs were conducted to detect the coefficients of determination (R^2). This data was used to conduct the QTL analysis. The QTL analysis was based on the Student's t-test of mean differences between each CSSL and the parent, Curinga (CSSL finder, Lorieux, 2005). The six VIs and the six yield related traits were used. The QTL detection was performed using both temporal replications, with a significance threshold of $P < 0.001$ applied to avoid false positives. Genotypic data sets consisting of 238 BeadXpress SNP markers (Thomson et al., 2012) were generated in the McCouch lab at Cornell University. Rough linkage maps were constructed from the SNP data using CSSL Finder v. 0.91 (Lorieux, 2005).

Results

3.1. Spatial and temporal variation in SR and yield related traits at harvest.

Fig. 4 shows examples of the spatial and temporal variation in Simple Ratio (SR) derived from the remote sensing system in the 2012 experiment. In the figure, the six yield related traits at harvest were also shown. SR reflects time series of rice greenness conditions. In the vegetative phase from EV to PI, SR increased with the increase of greenness within the rice canopy. SR peaked during PI, after which it decreased through FL to DG. Yield related traits, except for GS, showed significant differences among N treatments (Table 3). Increased N application rates had a positive effect on the SR values with regards to LV, PI, and FL.

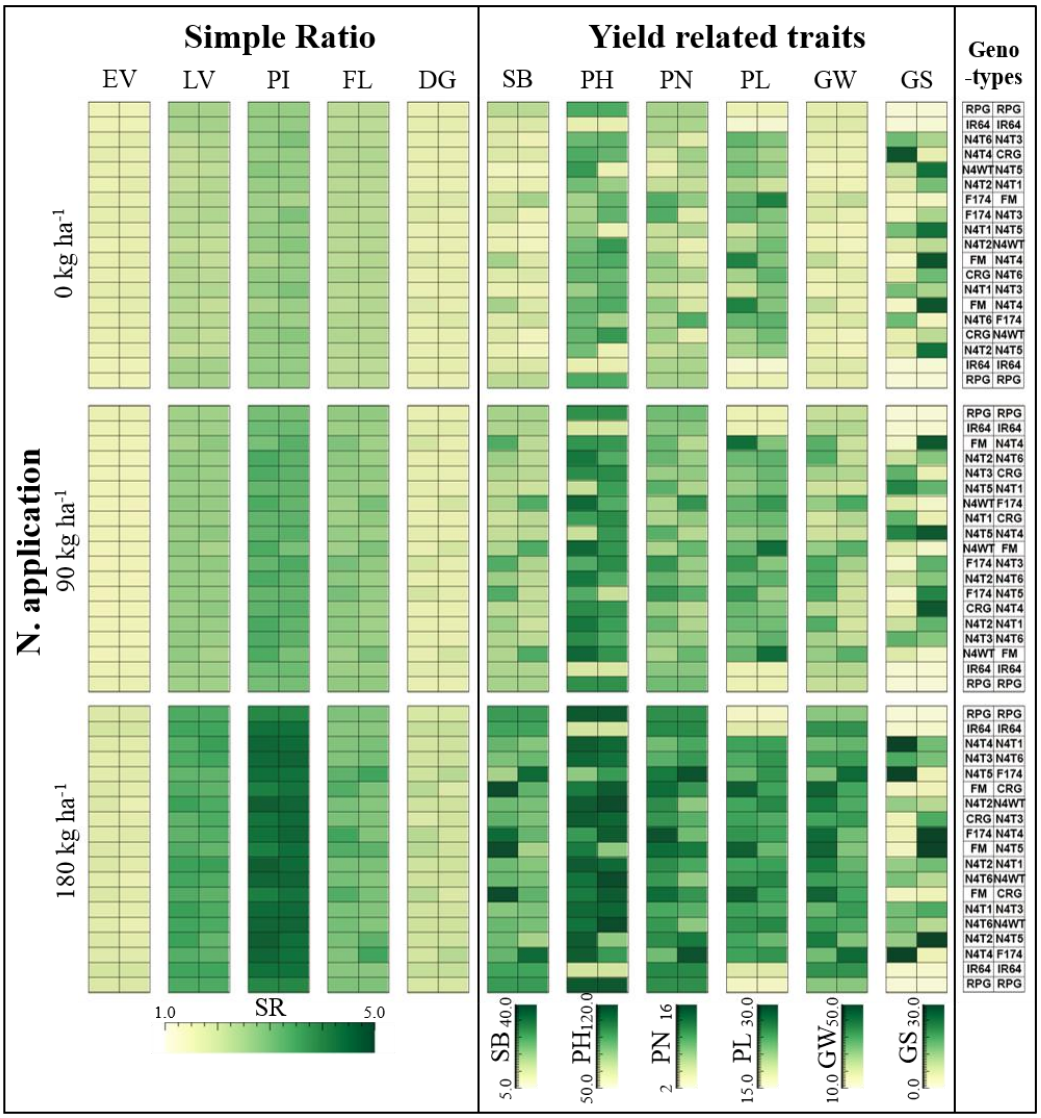

Fig. 4. Spatial and temporal variation in Simple Ratio (SR) and yield related traits at harvest in the 2012 experiment. SR is a vegetation index derived from the remote sensing images. Each SR indicated the values calculated from averaged reflectance on each plot for statistical analysis. Six yield related traits represents as follows; shoot biomass (SB), plant height (PH), panicle number (PN), panicle length (PL), grain weight (GW), and grain sterility percentage (GS). Genotypes indicated the plot position of genotypes in the 2012 experiment. Each abbreviation represents; Fedearroz 174 (F174), Fedearroz Mokari (FM), CRG (Curinga), RPG (*O. rufipogon*), IR64 (IR-64), N4 (NERICA 4) including wild type (WT) and transgenic lines (T).

3.2. The R^2 values of 11 VIs and CC versus yield related traits at flowering stage

For 11 VIs and CC versus six yield related traits at flowering in the 2012 and 2013 experiment, R^2 values are shown in Fig. 5. Among the six yield related traits tested SB, PN, and GW showed higher R^2 values, which indicated that these three yield related traits are possibly estimable by this system. The other three traits (GS, PH, and PL) showed considerably lower R^2 values, indicating that estimation of these traits may not possible by our system.

With regards to the three promising yield related traits (SB, PN, and GW), soil-line based VIs (PVI, TSAVI, and WDVI) were often worse than non soil-line based VIs. Adding to this, the R^2 values of the soil-line based VIs greatly varied between the two experiments. As expected, TVI and CTVI behaved similarly to NDVI and SR, since these indices were modified form of NDVI by definition. Compared to NDVI, GNDVI showed lower R^2 values in the 2012 experiment. However, it showed a similar result in the 2013 experiment. The R^2 values of SAVI and MSAVI were similar to NDVI, but their ability to estimate shoot biomass and panicle numbers were found to be lower in the 2012 experiment and higher in the 2013 experiment than NDVI.

At the flowering stage, CC indicated worse R^2 results than other VIs in most of the yield related traits and experiments.

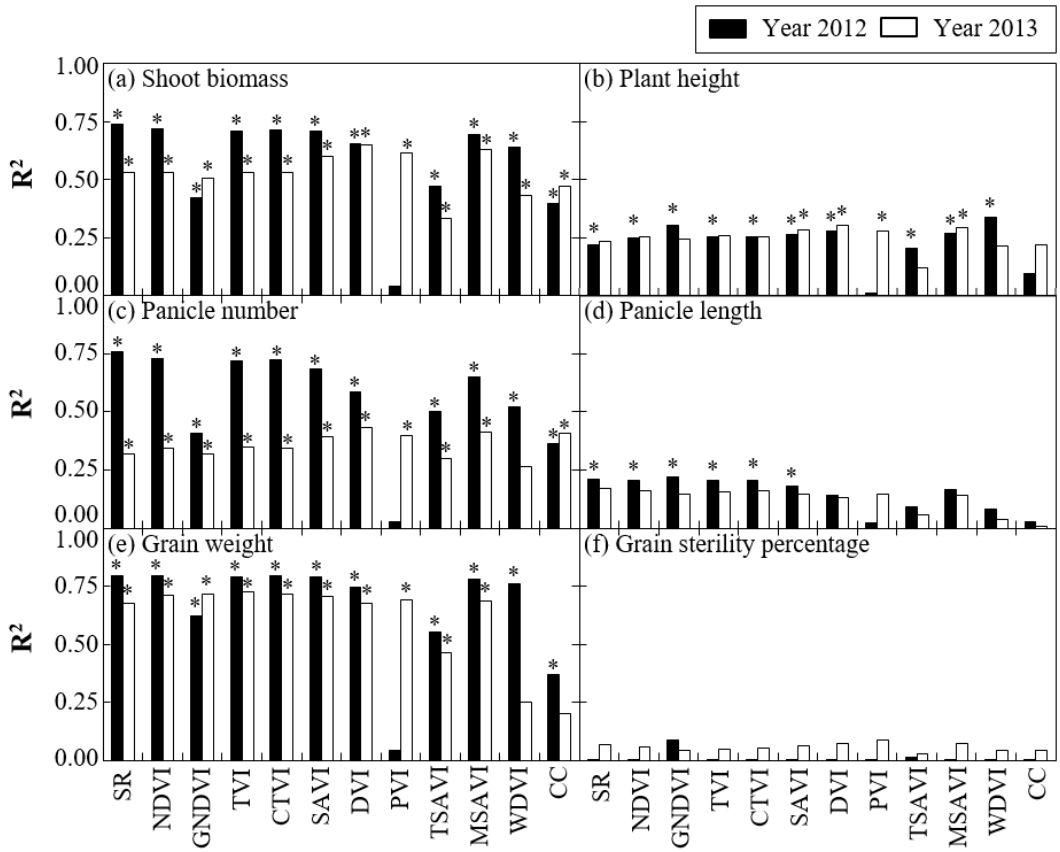

Fig. 5. The coefficient of determination (R^2) for 11 VIs and CC versus six yield traits at flowering stage in the 2012 and 2013 experiment. The bar colors represent the difference of two experiment; black bars represent the 2012 experiment and white bars represent the 2013 experiment. Statistical analyses were performed by using linear regression analysis: * represents significant at 0.01 level and no symbol means no significance.

3.3. The time series of R^2 values of VIs and CC versus grain weight during the rice growing stages.

Fig. 6 shows the time series of R^2 for the VIs and CC versus GW during the 2012 experiment (a, b, and c) and 2013 experiment (d, e, and f).

Fig. 6 (a), (b), and (c) shows the results of the 2012 experiment. For VIs without soil line parameters (Fig. 6 (a) and (b)), the result of NDVI, TVI, and CTVI were similar to SR. The R^2 values of these indices consistently increased during the vegetative phase from EV to LV and remained relatively unchanged until the DG stage (from 0.7 to 0.8 in R^2). DVI, SAVI, and MSAVI did not show differences with SR and NDVI after the late vegetative phase. However, at early vegetative phase, DVI, SAVI, and MSAVI showed about 0.2 or 0.3 higher R^2 than SR and NDVI. From the viewpoint of applied color bands, NDVI showed better results than GDVI during the crop life cycle.

In the results of the soil line based VIs (Fig. 6 (c)), WDVI and TSAVI resulted in the highest R^2 values from EV to LV as well as for DVI. After LV, WDVI showed similar changes to VIs without soil line parameters in Fig. 6 (a, b). On the other hand, The R^2 values of TSAVI kept about 0.6. PVI was generally unstable during all growth stages as compared to TSAVI and WDVI. Especially PVI had the lowest R^2 value, because we could not obtain appropriate soil line parameters at flowering in the 2012 experiment. PVI and TSAVI rarely showed higher R^2 values than that of WDVI or VIs without soil line parameters. The R^2 values of CC were lower than that of VIs during almost all growth stages.

Fig. 6 (d, e, and f) shows the time series of R^2 for nine VIs and CC versus GW in the 2013 experiment. For the VIs without soil line parameters (Fig. 6 (d) and (e)), all

VIs had the same trends of R^2 unlike the 2012 experiment; R^2 values increased during vegetative phase and reached the peak at reproductive phase around FL, then it dropped down after ripening phase (DG and MTG). The common characteristics of VIs between 2012 and 2013 experiment is that almost all of VIs without soil line parameters showed high R^2 values in DG and MTG. During the growth period, the R^2 peaks of VIs were at the same flowering times between the both experiments.

For soil-line based VIs (PVI, TSAVI and WDVI), R^2 values were unstable and greatly changed depending on the growth stage (Fig. 6 (f)). These characteristics are the same with that of the 2012 experiment. In the 2013 experiment, the R^2 of CC during vegetative phase was worse than the VIs in similar with the 2012 experiment.

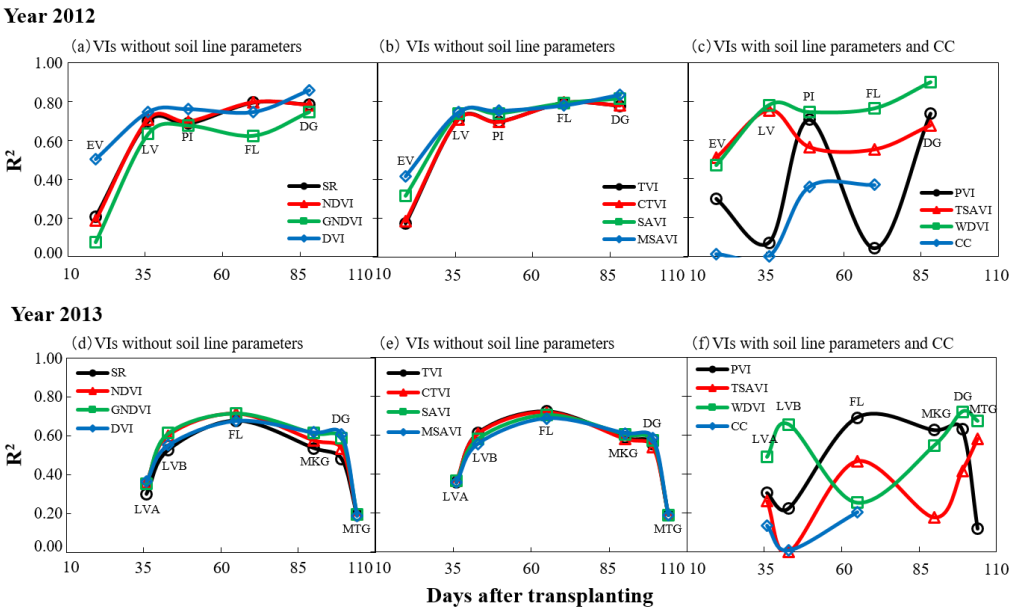

Fig. 6. Time series of the coefficient of determination (R^2) for nine VIs and CC versus grain weight in the 2012 (a, b, c) and 2013 (d, e, f) experiment. (a, b, d, e) The results of VIs without soil line parameters are shown. (c, f) The results of soil line based VIs and CC are shown. In the all figures, R^2 were calculated from grain weight at harvest versus VIs at several imaging times during rice growing stages. The imaging times were follows; in the 2012 experiment, early vegetative phase (EV, DAT 19), late vegetative phase (LV, DAT 35), panicle initiation (PI, DAT 49), flowering stage (FL, DAT 70), and dough grain stage (DG, DAT 88), and in the 2013 experiment, late vegetative phase -A (LVA, DAT 36), late vegetative phase -B (LVB, DAT 43), flowering stage (FL, DAT 65), milk grain stage (MKG, DAT 81), dough grain stage (DG, DAT 90), and mature grain stage (MTG, DAT 99).

3.4. The R^2 for VIs versus grain weight at the reproductive phases

From the results of *3.3*, it is confirmed that VIs obtained at reproductive phases (panicle initiation, flowering and milk grain stage) were promising indicators for grain weight estimation in both experiments. Fig. 7 (a) shows the R^2 for 11 VIs and CC versus GW at PI (2012), FL (2012 and 2013), and MKG (2013).

Among the combination of the 11 VIs and CC with three growth stages, SR, NDVI, TVI, CTVI, SAVI, and MSAVI exhibited higher correlation at flowering stage in both experiments. These VIs had similar performance during the growth stages. Above all, SR at FL (2012) indicated the highest R^2 value (0.80) during the reproductive phases (Fig. 7 (b)). The R^2 values of SR at the other growth stages were also higher; 0.69 at PI (2012) and 0.54 at MKG (2013).

In general, R^2 values of the 2012 experiment were higher than 2013 in all the crop stages studied. In 2012, DVI indicated lower R^2 values at FL but showed relatively higher R^2 values at PI. The R^2 values of soil-line based VIs (PVI, TSAVI, and WDVI) were unstable and varied widely depending on the growth stage. WDVI had a good correlation to yield related traits in 2012, but the correlation was poor in the 2013 experiment. There were some differences among visible bands using the NDVI formula. The R^2 values of GNDVI were lower than NDVI throughout the crop stages in the both experiments.

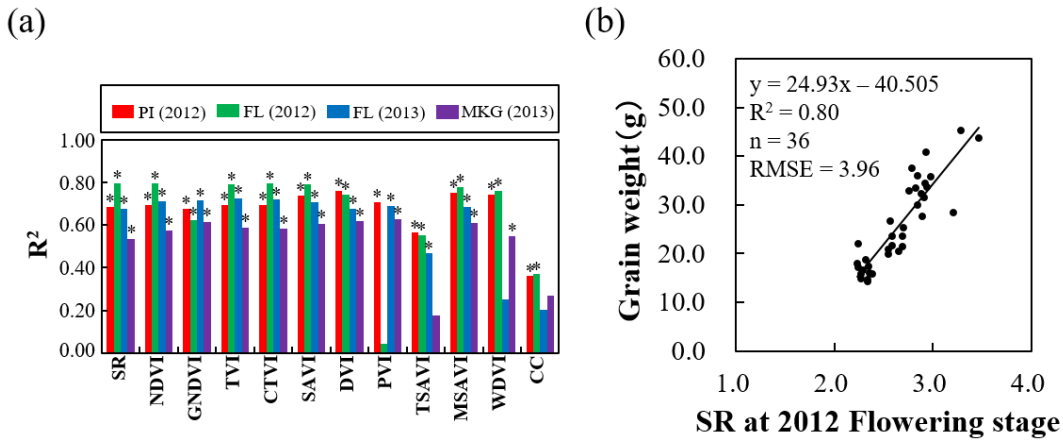

Fig. 7. (a) The coefficient of determination (R^2) for 11 VIs and CC at panicle initiation (2012), flowering stage (2012, 2013), and milk grain stage (2013) versus grain weight. Statistical analyses were performed by using linear regression analysis: * represents significant at 0.01 level and no symbol means no significance. (b) The scatter plot between grain weight at harvest and SR at flowering in the 2012 experiment.

3.5. Estimation of grain weight with response to different N application by using SR at flowering stage in the 2012 experiment

To show VI's ability to estimate GW at harvest, an example of the analysis is shown in Fig. 8. This analysis is based on SR obtained at FL and GW under different N treatments, the graph shows the response of genotypes on GW with different N applications in 2012. A One-way factorial ANOVA and multiple comparisons were performed to study the differences between N applications on GW and SR, respectively.

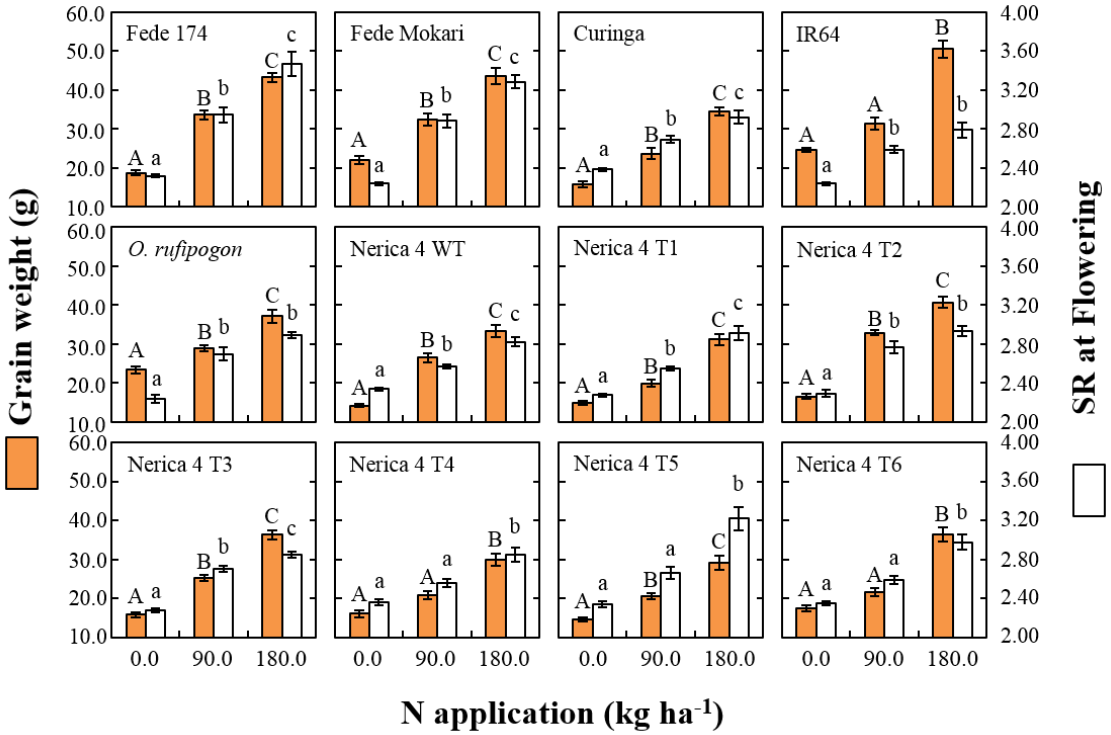

Fig. 8. The response of grain weight at harvest and SR at flowering stage to different N applications in the 2012 experiment. Columns marked by different letters differ significantly at $P < 0.01$ by Tukey Kramer test. Error bars show the standard error of the mean.

From Fig. 8, it is clear that SR reflected the variations among different N treatments. The SR and GW indicated high correlation (R^2 = 0.80) and similar tendencies in different N applications in almost all genotypes; SR and GW increased in

response to increased N applications.

In the view of the variation among genotypes, GW was clearly different. SR also reflected the characteristics of several genotypes. For example, SR of Fedearroz 174 and Fedearroz Mokari were relatively higher than other genotypes at each N application, which implies the higher GW. In contrast, there were some exceptions. For instance, SR of IR64 tended to be relatively lower, although its GW was higher than the other genotypes studied. Similarly, SR of N4-T5 tended to be higher, in spite of its low GW.

The result of multiple comparisons on each genotype revealed that the ranks of SR and GW among N applications were consistent in most of the genotypes (Fedearroz 174, Fedearroz Mokari, Curinga, *O. rufipogon,* N4-WT, N4-T1, N4-T3, N4-T4, and N4-T6). Only a few genotypes showed inconsistency in rankings. SR of IR64, N4-T2 and N4-T5 could not detect differences in grain weight between FP and 50% FP.

3.6. QTLs identified by image-based field phenotyping system

For 2014, R^2 values between yield related traits and VIs indicated higher during the reproductive phase, a trend inline with the 2012 and 2013 results. Out of the yield related traits studied, GW and SB showed higher R^2 values at PI or FL than that of DG. R^2 values of GW at PI were highest, the values ranged from $0.28 < R^2 < 0.48$, $P<0.001$ with all detected VIs. On the contrary, R^2 values of the other traits were very low. Correlation among the six VIs (SR, NDVI, CTVI, SAVI, DVI, MSAVI) revealed a significant positive correlation ($P<0.001$).

In this study, we have identified a total of eight QTLs on chromosomes 4, 7, 8, 9, 11 and 12 using VIs derived from image-based method. Among them, six QTLs on chromosomes, 4, 8, 9, 11 and 12 were consistently identified by all VIs (Table 4). On the other hand, using conventional agronomic data, we found two QTLs for GW and PN on chromosomes 3 and 12, respectively. QTLs for SB, PH, PL, and GS were not identified in this study.

Interestingly, the detected panicle number QTL on chromosome 12 using yield related traits overlapped with QTLs identified using VIs at PI (Table 4). We have found a common QTL between two methods, but the other five QTLs on chromosomes 4, 8, 9, 11, 12 were detected only by the image method.

Table 4. List of QTLs identified by all VIs derived from FBP imaging system under different N conditions

Trait	Stage	Treatment	Chr.	Marker	Position (Mb)
VIs	Panicle initiation	Native	4	id4007444-id4011696	22.83-34.11
VIs	Panicle initiation	FP	12	id12001102-id12005677	2.43-16.74
VIs	Flowering	Native	8	id8004756- id8005810	17.94-21.18
VIs	Flowering	FP	9	id9000233-id9000580	0.88-10.75
VIs	Flowering	FP	11	id11001777-id11005855	15.81-18.69
VIs	Flowering	FP	12	id12006190-id12008796	18.59-24.85
Grain weight	Harvesting	FP	3	id3002476-id3004123	4.32-7.68
Panicle number	Harvesting	FP	12	id12003803-id12005677	9.54-16.74

Discussion

In this study, we discuss an easy-to-deploy and tower-based phenotyping system as well as the performance of phenotyping by multispectral imaging devices under a field environment. Using this constructed field phenotyping system, we examined six yield related traits of rice (panicle number, grain weight, shoot biomass, grain sterility percentage, plant height, and panicle length). Although only the upper side of the canopy structure was visible from the towers and treated as the analysis region in our image processing system, the three important yield related traits (panicle number, grain weight, and shoot biomass) resulted in being estimable. No correlation between grain sterility percentage or panicle length was found with any VIs, because our system lacked the spatial resolution to discriminate the panicle or flowers in detail. Since this system sensed only upper plane of rice canopy, it was very difficult to acquire the information of plant height. In addition, the different imaging directions (Fig. 2 (b)) may affect the estimation of plant height. Estimation of plant height would be possible if we included canopy size as an analysis input. The structure from motion (Díaz-Varela et al., 2015), multi-view stereovision (Zhang et al., 2016), or 3D lidar techniques (Omasa et al., 2007; Lin, 2015) might enable this system to estimate plant height.

CC has the potential to represent plant growth development at early growth stages (Li et al., 2010). However, in our study it showed the worse performance of all of the VIs. The different image orientations from the towers may have been the cause, as CC is normally derived from field images taken from nadir. The oblique angle caused variations in spatial resolution across the study area. Because of the low pixel resolution, segregation between plant and non-plant regions was not possible from the towers.

As for the VI's formulas, vegetation indices with soil line parameters (PVI, TSAVI,

and WDVI) did not result in useful tools for estimation. As for soil-line based VIs, the parameters would be remarkably affected by the conditions of the sampled soil for soil-line regression. Therefore, it was difficult to draw the soil line appropriately every time since the field environment changes the surface based on the availability of irrigation water. The bidirectional reflectance distribution function (BRDF) effect may have caused this poor performance of soil-line based VIs. PVI, TSAVI and WDVI had no function to cancel the BRDF effect in their formulas.

The results of the modified indices (TVI and CTVI) were similar to the original NDVI in this study, which means that NDVI was sufficient for yield estimation from the viewpoint of simplicity of the calculation. The similar performance of the modified indices is not surprising in this experimental set up, because the variations of most of the agronomical traits were artificially generated by different N fertilizations.

In the estimation of grain weight NDVI exhibited better performance than GNDVI. This might be attributed to the ability of the red band to register differences among some vegetation properties which were not discernable in the green band. Gitelson et al., (1996) reported that the green band exhibits a wider range of chlorophyll sensitivity than the red band under dense leaf or pigment conditions. Possible causes of this discrepancy in findings may include the broad sensible wavelength of the green channel in the commercial RGB camera used (i.e. red and blue light effects the green channel) and/or the low leaf density of our rice plots.

In terms of grain weight estimation, the most appropriate time to take images was around flowering (Fig. 6 and Fig. 7). This result agrees with previous work (Mosleh et al., 2015), which confirms that our imaging system is functioning normally. Earliness of rice growth may cause the increase of R^2 in the flowering. From the perspective of

earliness, late flowering cultivars result in better yield performance than early flowering cultivars. In the 2012 experiment, late flowering cultivars kept the greenness at flowering time, while early flowering cultivars decreased canopy greenness with the progression of the flowering. Therefore, it seems that VIs effectively detected the higher yielding cultivars. From this result, the timing of image capture is very important for the performance of rice yield traits estimation.

SR at flowering stage of the 2012 experiment exhibited the best performance to estimate the grain weight at harvest (R^2=0.80) throughout all the experiments. This value is close to the result found by Swian et al., 2010 where they used an aerial platform and NDVI to estimate rice yield (R^2=0.76) at a mid-growth stage. Furthermore, the R^2 value of this study is higher than the result of a NDVI regression model obtained through the use of the Green Seeker sensor (R^2=0.36; panicle initiation and R^2=0.42; panicle differentiation) reported by Harrell et al. 2011. Results of 2013 experiment showed that R^2 of VIs increased throughout the growth stage and reached a peak during the reproductive phase (flowering and milk grain stage), then the R^2 dropped after the ripening phase (dough grain stage and mature grain stage). Rice canopies around flowering time reflect the situation of rice plant with higher chlorophyll content in the shoot, which may improve the correlation. The reason why R^2 decreased after the ripening phase is related to the senescence of plant leaves. In the 2012 experiment (Fig. 4), R^2 of vegetation indices did not decrease because we did not capture the images after dough grain stage.

At the flowering stage SR, NDVI, TVI, CTVI, SAVI, and MSAVI suggested an ability to estimate grain weight in spite of differences in growth conditions between the 2012 and 2013 experiments. In fact, there were some differences between the two

experiments; plot size, replicates used for image analysis, environmental factors like temperature, precipitation and radiation. Notably, higher radiation and rainfall was observed in the 2013 experiment. These environmental conditions potentially created variations in response to N treatments between the experiments. The R^2 values in the 2012 experiment were higher than 2013 (Fig. 5). There are two possible causes for this difference. The first one is the number of replications used for image analysis. In 2012, we used three replicates to estimate yield traits using VIs, while in 2013 only two replicates were used. The second reason may relate to the genetic nature of genotypes used in the experiments. In 2012, out of 12 lines studied, seven were derived from similar background that is NERICA4. These transgenic lines were homozygous and differed in only one gene. On the other hand, in 2013 experiment we used diverse lines compared to 2012. Therefore, flowering and maturity patterns among the lines were different. Even though we tried our best to homogenize the flowering time between the genotypes in 2013, the developmental phenology varied between the genotypes. We believe this technology can be useful in situations where the lines are from similar genetic backgrounds. Although there was a significant difference in overall agronomic performance between the experiments, indices namely SR, NDVI, TVI, CTVI, SAVI and MSAVI exhibited consistent performance.

In comparison of the QTL results from the two different phenotyping methods (image and conventional- ground truth data), we found that the image based phenotyping method proved more accurate than conventional methods in the dissection of complex traits. Furthermore, traditional phenotypic measurements did not have sufficient power to study relatively complex traits such as shoot biomass.

In this study, the region of the identified QTLs on chromosome 12 using VIs at

panicle initiation overlapped with QTLs for panicle number identified using ground truth agronomic data. This clearly implies that a developed phenotyping system can be useful in the identification of QTLs and may lead to gene discovery. However, QTLs detected on chromosome 4, 8, and 9 (dry season experiment, February to June in 2014) by VIs were not present in the QTL analysis using ground truth agronomic data. Interestingly, these three QTLs overlapped with the QTL regions for shoot biomass on chromosome 4, SPAD values on chromosome 8, and panicle number on chromosome 9. These findings are in line with those reported by Ogawa et al., 2016 in the same environment. The co-location of QTLs across the genetic background in rice was previously reported in tiller number on chromosome 4 (Zhou et al., 2013) and chromosome 12 (Wissuwa et al., 1998).

Our study clearly demonstrates that to dissect the variation in complex traits like grain weight and shoot biomass, the image based method is the better option compared to the conventional QTL analysis based on ground truth agronomic data. Compared to traditional phenotyping, the image-based method represents a novel real time monitoring tool that can facilitate major advances in plant functional genomics and crop breeding. These results clearly demonstrate that the image-based method has a potential to detect QTLs which cannot be identified by conventional QTL analysis. In the future, the TBFPS imaging system might be used to map the QTLs for different abiotic stresses. Considering the relatively small population size and the fact that separating QTL-by-N treatment interaction was not possible, the results must be regarded as preliminary and further validation is required.

Conclusions

We examined the tower derived VIs to estimate rice yield components of different rice genotypes using commonly available commercial SLR cameras. This study supports the use of crop images to predict yield and yield related traits prior to harvest. The main contributions of this research are: 1) our results suggest the best physiological stage for capturing images is around flowering, 2) some promising indices (SR, NDVI, TVI, CTVI, SAVI, and MSAVI) correlated to grain weight in spite of the differences of the growth conditions, 3) SR at flowering stage can correlate to grain weight at harvest (R^2 is 0.80), and 4) we identified the QTL region regulating panicle number under different N treatments using this imaging system.

Based on these results, this TBFPS could help us screen a large number of germplasm against various biotic and abiotic stresses based on the yield performance. However, as environmental conditions change, for example under drought, we would need to further validate the system. In the future, it might be possible to automate much, if not all, of the image processing. Unsupervised image processing is necessary for automated HTP and scaling up to the large datasets. Especially computer-based plot area assignment may be essential function to realize fully automated HTP for this study. Additionally, arranging web-based software will allow crop breeders to operate HTP analyses more rapidly. Real time field based HTP monitoring system demonstrated in this study will hopefully address some of the environmental and sustainable agricultural challenges the world is facing.

Acknowledgements

We thank Richard Bruton, Research scholar at Texas A&M for a critical evaluation and editing of this manuscript. Transgenic rice lines in this study was provided by Arcadia Biosciences, Davis, CA, USA, the Funding for generating transgenic lines African Agricultural Technology Foundation (AATF) through USAID's "Feed the Future" initiative. We thank Dr. Susan McCouch and Juan David Arbelaez at Cornell University for providing SNP data sets and Dr. Mathias Lorieux at Institut de Recherche pour le Développement (IRD) for providing CSSLs seed. We thank Dr. Joe Tohme, Agro biodiversity research area director CIAT for his continuous support. We also thank Ministry of Foreign Affairs of Japan (MOFA) and JICA for the financial support to perform this study and a part of this study was conducted as SATREPS project (JICA-JST).

References

Alexandersson, E., Jacobson, D., Vivier, M. A., Weckwerth, W., Andreasson, E., 2014. Field-omics – understanding large-scale molecular data from field crops. Frontiers in Plant Science 5, 286.

Andrade-Sanchez, P., Gore, M. A., Heun, J. T., Thorp, K. R., Carmo-Silva, A. E., French, A. N., Salvucci, M. E., White, J. W., 2014., Development and evaluation of a field-based high-throughput phenotyping platform. Functional Plant Biology 41, 68-79.

Araus, J. L., Cairns, J. E., 2014. Field high-throughput phenotyping: the new crop breeding frontier. Trends in Plant Science 19(1), 52-61.

Baret, F., Guyot, G., 1991. Potentials and limits of vegetation indices for LAI and APAR assessment. Remote Sensing of Environment 35(2), 161-173.

Barmeier, G., Schmidhalter, U., 2016. High-Throughput Phenotyping of Wheat and Barley Plants Grown in Single or Few Rows in Small Plots Using Active and Passive Spectral Proximal Sensing. Sensors 16(11), 1860.

Behmann, J., Mahlein, A. K., Paulus, S., Kuhimann, H., Oerke, E. C., Plümer, L., 2015. Calibration of hyperspectral close-range pushbroom cameras for plant phenotyping. ISPRS Journal of Photogrammetry and Remote Sensing 106, 172-182.

Birth, G. S., McVey, G. R., 1968. Measuring the color of growing turf with a reflectance spectrophotometer. Agronomy Journal 60(6), 640-643.

Chapman, S. C., Merz, T., Chan, A., Jackway, P., Hrabar, S., Dreccer, M. F., Holland, E., Zheng, B., Ling, T. J., Jimenez-Berni, J., 2014. Pheno-Copter: a low-altitude, autonomous remote-sensing robotic helicopter for high-rhroughput field-based phenotyping. Agronomy 4, 279-301.

Clevers, J. G. P. W., 1988. The derivation of a simplified reflectance model for the estimation of leaf area index. Remote Sensing of Environment 25(1), 53-69.

Colomina, I., Molina, P., 2014. Unmanned aerial systems for photogrammetry and remote sensing: A review. ISPRS Journal of Photogrammetry and Remote Sensing 92, 79-97.

Deery, D., Jimenez-Berni, J., Jones, H., Sirault, X., Furbank, R., 2014. Proximal remote sensing buggies and potential applications for field-based phenotyping. Agronomy 4(3), 349-379.

Derring, D. W., Rouse, J. W., Haas, R. H., Schell, H. H., 1975. Measuring "forage production" of grazing units from Landsat MSS data. Proceedings of the Tenth International Symposium of Remote Sensing of the Environment, ERIM, ANN Arbor, Michigan, 1169-1198.

Díaz-Varela, R. A., Rosa, R., León, L., Zarco-Tejada, P. J., 2015. High-resolution airborne UAV imagery to assess olive tree crown parameters using 3D photo reconstruction: application in breeding trials. Remote Sensing 7(4), 4213-4232.

Edae, E. A., Byrne, P. F., Haley, S. D., Lopes, M. S., Reynolds, M. P., 2014. Genome-wide association mapping of yield and yield components of spring wheat under contrasting moisture regimes. Theoretical and Applied Genetics 127(4), 791-807.

Fiorani, F., Schurr, U., 2013. Future scenarios for plant phenotyping. Annual Reviews of Plant Biology 64, 267-291.

Furbank, R.T. (Eds), 2009. Plant phenomics: from gene to form and function. Functional Plant Biology 36(10 and 11), v-vi, 845-1026.

Gao, F., Wen, W., Liu, J., Rasheed, A., Yin, G., Xia, X., Wu, X., He, Z., 2015. Genome-wide linkage mapping of QTL for yield components, plant height and yield-related physiological traits in the Chinese wheat cross Zhou 8425B/Chinese Spring. Frontiers in Plant Science 6, 1099.

George, T. S., Hawes, C., Newton, A. C., McKenzie, B. M., Hallett, P. D., Valentine, T. A., 2014. Field phenotyping and long-term platforms to characterise how crop genotypes interact with soil processes and the environment. Agronomy 4(2), 242-278.

Gitelson, A. A., Kaufman, Y. J., Merzlyak, M. N., 1996. Use of a green channel in remote sensing of global vegetation from EOS-MODIS. Remote Sensing of Environment 58(3), 289-298.

Gonzalez-Dugo, V., Hernandez, P., Solis, I., Zarco-Tejada, P. J., 2015. Using high-resolution hyperspectral and thermal airborne imagery to assess physiological condition in the context of wheat phenotyping. Remote Sensing 7(10), 13586-13605.

Graziani, M., Maccaferri, M., Royo, C., Salvatorelli, F., Tuberosa, R., 2014. QTL dissection of yield components and morpho-physiological traits in a durum wheat

elite population tested in contrasting thermos-pluviometric conditions. Crop and Pasture Science 65(1), 80-95.

Haghighattalab, A., Pérez, L. G., Mondal, S., Singh, D., Schinstock, D., Rutkoski, J., Ortiz-Monasterio, I., Singh, R. P., Goodin, D., Poland, J., 2016. Application of unmanned aerial systems for high throughput phenotyping of large wheat breeding nurseries. Plant Methods 12(1), 35.

Harrell, D. L., Tubaña, B. S., Walker, T. W., and Phillips, S. B., 2011. Estimating rice grain yield potential using Normalized Difference Vegetation Index. Agronomy Journal 103(6), 1717-1723.

He, L., Song, X., Feng, W., Guo, B. B., Zhang, Y. S., Wang, Y. H., Wang, C. Y., Guo, T. C., 2016. Improved remote sensing of leaf nitrogen concentration in winter wheat using multi-angular hyperspectral data. Remote Sensing of Environment 174, 122-133.

Henry, A., Swamy, B. P. M., Dixit, S., Torres, R. D., Batoto, T. C., Manalili, M., Anantha, M. S., Mandal, N. P., Kumar, A., 2015. Physiological mechanisms contributing to the QTL-combination effects on improved performance of IR64 rice NILs under drought. Journal of Experimental Botany 66(7), 1787-1799.

Honsdorf, N., March, T. J., Berger, B., Tester, M., Pillen, K., 2014. High-throughput phenotyping to detect drought tolerance QTL in wild barley introgression lines. PLOS ONE 9(5), e97047.

Huete, A. R., 1988. A soil-adjusted vegetation index (SAVI). Remote Sensing of Environment 25(3), 295-309.

Inostroza, L., Acuña, H., Munoz, P., Vásquez, C., Ibáñez, J., Tapia, G., Pino, M. T., Aguilera, H., 2016. Using Aerial Images and Canopy Spectral Reflectance for High-Throughput Phenotyping of White Clover. Crop Science 56(5), 2629-2637.

Jones, H. G., Vaughan, R. A., 2010. Remote sensing of vegetation: principles, techniques, and publications. Oxford University Press, New York.

Khan, M. A., Saravia, D., Munive, S., Lozano, F., Farfan, E., Eyzaguirre, R., Bonierbale, M., 2015. Multiple QTLs linked to agro-morphological and physiological traits related to drought tolerance in potato. Plant Molecular Biology Repoter, 33(5), 1286-1298.

Kumar, S., Röder, M. S., Singh, R. P., Kumar, S., Chand, R., Joshi, A. K., Kumar, U.,

2016. Mapping of spot blotch disease resistance using NDVI as a substitute to visual observation in wheat (*Triticum aestivum* L.). Molecular Breeding 36(7), 1-11.

Li, L., Zhang, Q., Huang, D., 2014. A review of imaging techniques for plant phenotyping. Sensors 14(11), 20078-20111.

Li, X. M., Chen, X. M., Xiao, Y. G., Xia, X. C., Wang, D. S., He, Z. H., Wang, H. J., 2014. Identification of QTLs for seedling vigor in winter wheat. Euphytica 198(2), 199-209.

Li, X. M., He, Z. H., Xiao, Y. G., Xia, X. C., Trethowan, R., Wang, H. J., Chen, X. M., 2015. QTL mapping for leaf senescence-related traits in common wheat under limited and full irrigation. Euphytica 203(3), 569-582.

Li, Y., Chen, D., Walker, C. N., Angus, J. F., 2010. Estimating the nitrogen status of crops using a digital camera. Field Crops Research 118(3), 221-227.

Lin, Y., 2015. LiDAR: An important tool for next-generation phenotyping technology of high potential for plant phenomics?. Computers and Electronics in Agriculture 119, 61-73.

Liebisch, F., Kirchgessner, N., Schneider, D., Walter, A., Hund, A., 2015. Remote, aerial phenotyping of maize traits with a mobile multi-sensor approach. Plant Methods 11, 9.

Lorieux, M., 2005. CSSL Finder: a free program for managing introgression lines, http://mapdisto.free.fr/.

Lu, Y., Xu, J., Yuan, Z., Hao, Z., Xie, C., Li, X., Shah, T., Lan, H., Zhang, S., Rong, T., Xu, Y., 2012. Comparative LD mapping using single SNPs and haplotypes identifies QTL for plant height and biomass as secondary traits of drought tolerance in maize. Molecular Breeding 30(1), 407-418.

Merewitz, E. B., Belanger, F. C., Warnke, S., E., Huang, B., 2012. Identification of quantitative trait loci linked to drought tolerance in a colonial × creeping bentgrass hybrid population. Crop Science 52(4), 1891-1901.

Merewitz, E., Belanger, F., Warnke, S., Huang, B., Bonos, S., 2014.Quantitative trait loci associated with drought tolerance in creeping bentgrass. Crop Science 54(5), 2314-2324.

Moharana, S., Dutta, S., 2016. Spatial variability of chlorophyll and nitrogen content of

rice from hyperspectral imagery. ISPRS Journal of Photogrammetry and Remote Sensing 122, 17-29.

Mosleh, M. K., Hassan, Q. K., Chowdhury, E. H., 2015. Application of remote sensors in mapping rice area and forecasting its production: a review. Sensors 15(1), 769-791.

Obsa, B. T., Eglinton, J., Coventry, S., March, T., Langridge, P., Fleury, D., 2016. Genetic analysis of developmental and adaptive traits in three doubled haploid populations of barley (*Hordeum vulgare* L.). Theoretical and Applied Genetics 129(6), 1139-1151.

Ogawa, S., Selvaraj, M. G., Fernando, A. J., Lorieux, M., Ishitani, M., McCouch, S., Arbelaez, J. D., 2014a. N- and P- mediated seminal root elongation response in rice seedlings. Plant and Soil 375(1), 303-315.

Ogawa, S., Valencia, M. O., Ishitani, M., Selvaraj, M. G., 2014b. Root system architecture variation in response to different $NH4^{+}$ concentrations and its association with nitrogen-deficient tolerance traits in rice. Acta Physiologiae Plantarum 36(9), 2361-2372.

Ogawa, S., Valencia, M. O., Lorieux, M., Arbelaez, J. D., McCouch, S., Ishitani, M., Selvaraj, M. G., 2016. Identification of QTLs associated with agronomic performance under nitrogen-deficient conditions using chromosome segment substitution lines of a wild rice relative; *Oryza rufipogon*. Acta Physiologiae Plantarum 38(4), 1-10.

Omasa, K., 1990. Image instrumentation methods of plant analysis. In: Linskens, H.F., Jackson, J.F. (Eds) Modern methods of plant analysis. Springer-Verlag, Berlin, 203-243.

Omasa, K., Saji, H., Youssefian, S., Kondo, N. (Eds), 2002. Air pollution and plant biotechnology. Springer-Verlag, Tokyo.

Omasa, K., Hosoi, F., Konishi, A., 2007. 3D lidar imaging for detecting and understanding plant responses and canopy structure. Journal of Experimental Botany 58(4), 881-898.

Otsu, N., 1975. A threshold selection method from gray level histograms. Automatica 11, 23-27.

Pauli, D., Andrade-Sanchez, P., Carmo-Silva, A. E., Gazave, E., French, A. N., Heun, J., Hunsaker, D. J., Lipka, A. E., Setter, T. L., Strand, R. J., Thorp, K. R., Wang, S., White, J. W., Gore, M. A., 2016. Field-based high throughput plant phenotyping reveals the temporal patterns of quantitative trait loci associated with stress-responsive traits in cotton. G3-Genes Genomes Genetics 6(4), 865-879.

Perry, C. Jr., Lautenschlager, L. F., 1984. Functional equivalence of spectral vegetation indices. Remote Sensing of Environment 14(1-3), 169-182.

Pieruschka, R., Lawson, T. (Eds), 2015. Phenotyping in plants. Journal of Experimental Botany 66(18), 5385-5637.

Pinto, R. S., Reynolds, M. P., Mathews, K. L., McIntyre, C. L., Olivares-Villegas, J., Capman, S. C., 2010. Heat and drought adaptive QTL in a wheat population designed to minimize confounding agronomic effects. Theoretical and Applied Genetics 121(6), 1001-1021.

Qi J., Chehbouni, A., Huete, A. R., Kerr, Y. H., Sorooshian, A., 1994. A modified soil adjusted vegetation index. Remote Sensing of Environment 48(2), 119-126.

Richardson, A. J., Wiegand, C. L., 1977. Distinguishing vegetation from soil background information. Photogrammetric Engineering and Remote Sensing 43(12), 1541-1552.

Rouse, J. W., Haas, R. H., Schell, J. A., Deering, D. W., Harlan J. C., 1974. Monitoring the vernal advancement and retrogradation (greenwave effect) of natural vegetation. NASA/GSFC Final report, Greenbelt, MD, USA.

Sankaran, S., Khot, L. R., Carter, A. H., 2015. Field-based crop phenotyping: Multispectral aerial imaging for evaluation of winter wheat emergence and spring stand. Computers and Electronics in Agriculture 118, 372-379.

Sakamoto, T., Shibayama, M., Kimura, A., Takada, E., 2011. Assessment of digital camera-derived vegetation indices in quantitative monitoring of seasonal rice growth. ISPRS Journal of Photogrammetry and Remote Sensing 66(6), 872-882.

Shibayama, M., Sakamoto, T., Takada, E., Inoue, A., Morita, K., Takahashi, W., Kimura, A., 2009. Continuous monitoring of visible and near-infrared band reflectance from a rice paddy for determining nitrogen uptake using digital cameras. Plant Production Science 12(3), 293-306.

Shibayama, M., Sakamoto, T., Takada, E., Inoue, A., Morita, K., Takahashi, W., Kimura, A., 2011. Estimating paddy rice leaf area index with fixed point continuous observation of near infrared reflectance using a calibrated digital camera. Plant Production Science 14(1), 30-46.

Shibayama, M., Sakamoto, T., Takada, E., Inoue, A., Morita, K., Yamaguchi, T., Takahashi, W., Kimura, A., 2012. Estimating rice leaf greenness (SPAD) using fixed-point continuous observations of visible red and near infrared narrow-band digital images. Plant Production Science 15(4), 293-309.

Silleos, N. G., Alexamdridis, T. K., Ioannis, Z. G., Perakis, K., 2006. Vegetation Indices: advances made in biomass estimation and vegetation monitoring in the last 30 years. Geocarto International 21(4), 21-28.

Sultana, S. R., Ali, A., Ahmad, A., Mubeen, M., Zia-Ul-Haq, M., Ahmad, S., Ercisli, S., Jaafar, H. Z. E., 2014. Normalized Difference Vegetation Index as a Tool for Wheat Yield Estimation: A Case Study from Faisalabad, Pakistan, The Scientific World Journal 2014, Article ID 725326.

Svensgaard, J., Roitsch, T., Christensen, S., 2014. Development of a mobile multispectral imaging platforms for precise field phenotyping. Agronomy 4(3), 322-336.

Swain K. C., Thomson, S. J., Jayasuriya, H. P. W., 2010. Adoption of an unmanned helicopter for low-altitude remote sensing to estimate yield and total biomass of a rice crop. Transactions of the ASABE 53(1), 21-27.

Tattaris, M., Reynolds, M. P., Chapman, S. C., 2016. A direct comparison of remote sensing approaches for high-throughput phenotyping in plant breeding. Frontiers in Plant Science 7, 1131.

Tubaña, B., Harrell, D., Walker, T., Teboh, J., Lofton, J., Kanke, Y., Phillips, S., 2011. Relationships of spectral vegetation indices with rice biomass and grain yield at different sensor view angles. Agronomy Journal 103(5), 1405-1413.

Thomson, M. J., Zhao, K., Wright, M., McNally, K. L., Rey, J., Tung, C. W., Reynolds, A., Scheffler, B., Eizeng, G., McClung, A., Kim, H., Ismail, A. M., Ocampo, M., Mojica, C., Reveche, M. Y., Dilla-Ermita, C. J., Mauleon, R., Leung, H., Bustamante, C., McCouch, S., 2012. High-throughput single nucleotide polymorphism genotyping for breeding applications in rice using the BeadXpress

platform. Molecular Breeding 29(4), 875–886.

Trachsel, S., Sun, D., SanVicente, F. M., Zheng, H., Atlin, G. N., Suarez, E. A., Babu, R., Zhang, X., 2016. Identification of QTL for Early Vigor and Stay-Green Conferring Tolerance to Drought in Two Connected Advanced Backcross Populations in Tropical Maize (*Zea mays* L.). PloS one 11(3), e0149636.

Trapp, J. J., Urrea, C. A., Zhou, J., Khot, L. R., Sankaran, S., Miklas, P. N., 2016. Selective Phenotyping Traits Related to Multiple Stress and Drought Response in Dry Bean. Crop Science 56, 1460-1472.

Tucker, C. J., 1979. Red and photographic infrared linear combinations for monitoring vegetation. Remote Sensing of Environment 8(2), 127-150.

Vadez, V., Kholová, J., Hummel, G., Zhokhavets, U., Gupta, S. K., Hash, C. T., 2015. LeasyScan: a novel concept combining 3D imaging and lysimetry for high-throughput phenotyping of traits controlling plant water budget. Journal of Experimental Botany 66(18), 5581-5593.

Wang, Y., Wang, D, Zhang, G., Wang, J., 2013. Estimating nitrogen status of rice using the image segmentation of G-R thresholding method. Field Crops Research 149(1), 33-39.

Wang, Y., Wang, D., Shi, P., Omasa, K., 2014. Estimating rice chlorophyll content and leaf nitrogen concentration with a digital still color camera under natural light. Plant Methods 10, 36.

White, J. W., Andrade-Sanchez, P., Gore, M. A., Bronson, K. F., Coffelt, T. A., Conley, M. M., Feldmann, K. A., French, A. N., Heun, J. T., Hunsaker, D. J.. 2012. Field-based phenomics for plant genetics research. Field Crops Research 133(11), 101-112.

White, J. W., Conley, M. M., 2013. A flexible, low-cost cart for proximal sensing. Crop Science 53(4), 1646-1649.

Wissuwa, M., Yano, M., Ae, N., 1998. Mapping of QTLs for phosphorus-deflciency tolerance in rice (Oryza Sativa L.). Theoretical and Applied Genetics 97(5), 777-783.

Yu, N., Li, L., Schmitz, N., Tian, L. F., Greenberg, J. A., Diers, B. W., 2016. Development of methods to improve soybean yield estimation and predict plant

maturity with an unmanned aerial vehicle based platform. Remote Sensing of Environment 187, 91-101.

Zaman-Allah, M., Vergara, O., Araus, J. L., Tarekegne, A., Magorokosho, C., Zarco-Tejada, P. J., Hornero, A., Albà A. H., Das, B., Craufurd, P., Olsen, M., Prasanna, B. M., Cairns, J., 2015. Unmanned aerial platform-based multi-spectral imaging for field phenotyping of maize. Plant Methods 11, 35.

Zarco-Tejada, P. J., González-Dugo, M. V., Fereres, E., 2016. Seasonal stability of chlorophyll fluorescence quantified from airborne hyperspectral imagery as an indicator of net photosynthesis in the context of precision agriculture. Remote Sensing of Environment 179, 89-103.

Zhang, Y., Teng, P., Shimizu, Y., Hosoi, F., Omasa, K., 2016. Estimating 3D Leaf and Stem Shape of Nursery Paprika Plants by a Novel Multi-Camera Photography System. Sensors 16(6), 874.

Zhou, S., Zhu, M., Wang, F., Huang, J., Wang, G., 2013. Mapping of QTLs for yield and its components in a rice recombinant inbred line population. Pakistan Journal of Botany 45(1), 183-189.

Figure

Click here to download Figure: Naito et al.pptx

Fig. 1

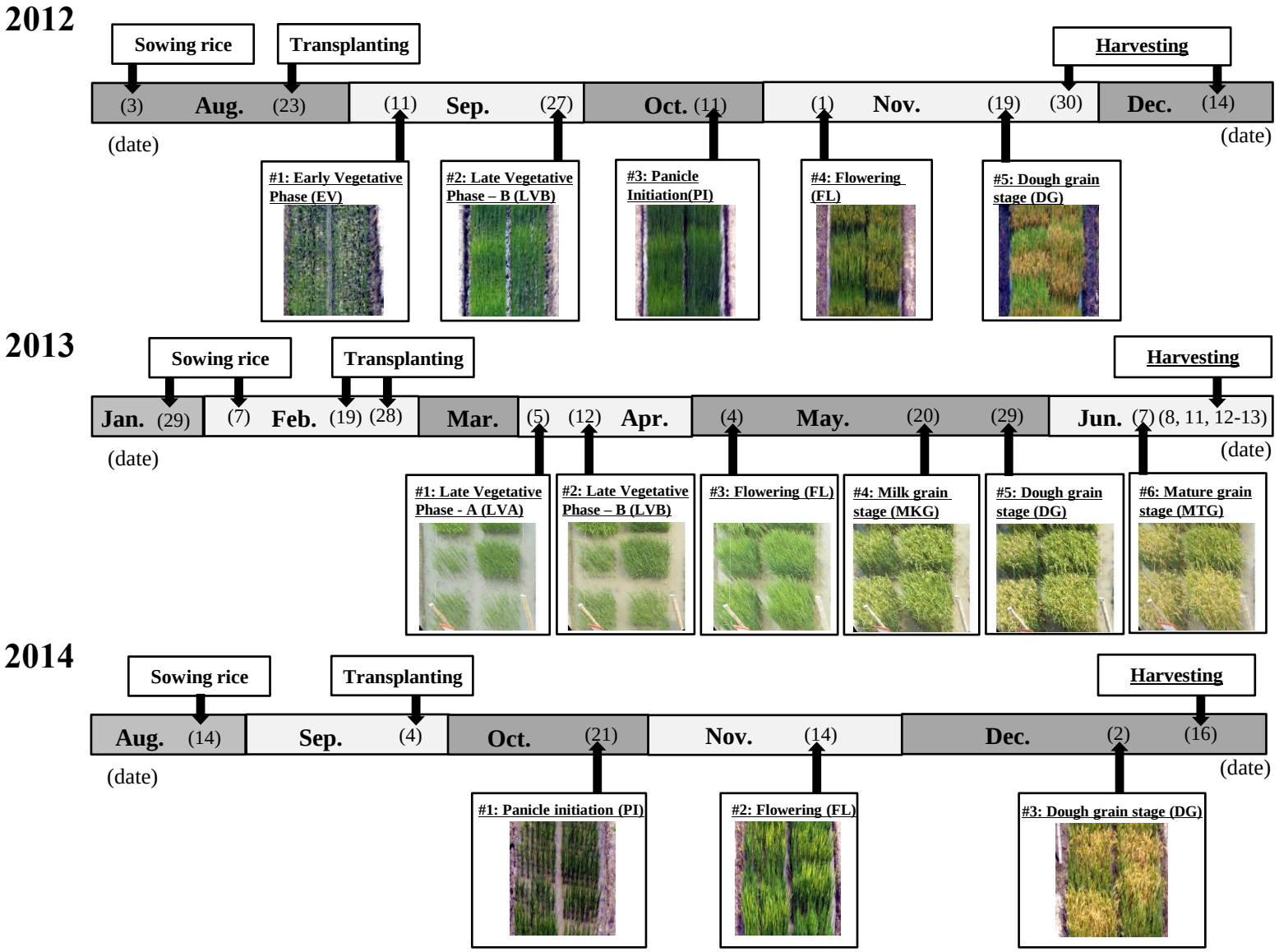

Fig. 2

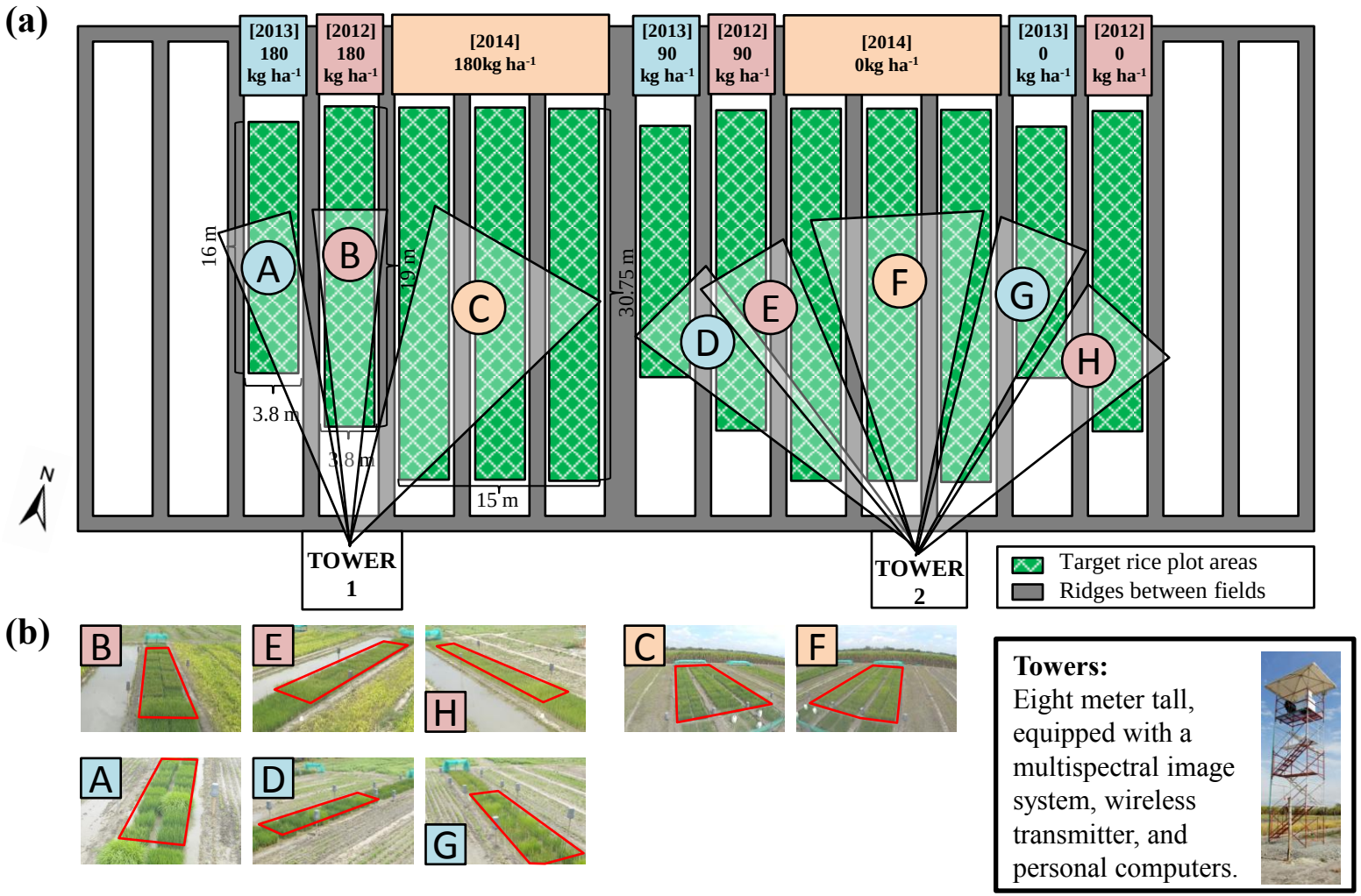
(a)
[2013] 180 kg ha-1
[2012] 180 kg ha-1
[2014] 180kg ha-1
[2013] 90 kg ha-1
[2012] 90 kg ha-1
[2014] 0kg ha-1
[2013] 0 kg ha-1
[2012] 0 kg ha-1
A
B
C
D
E
F
G
H
16 m
19 m
30.75 m
3.8 m
3.8 m
15 m
N
TOWER 1
TOWER 2
Target rice plot areas
Ridges between fields
(b)
B
E
H
C
F
A
D
G
Towers:
Eight meter tall, equipped with a multispectral image system, wireless transmitter, and personal computers.

Fig. 3

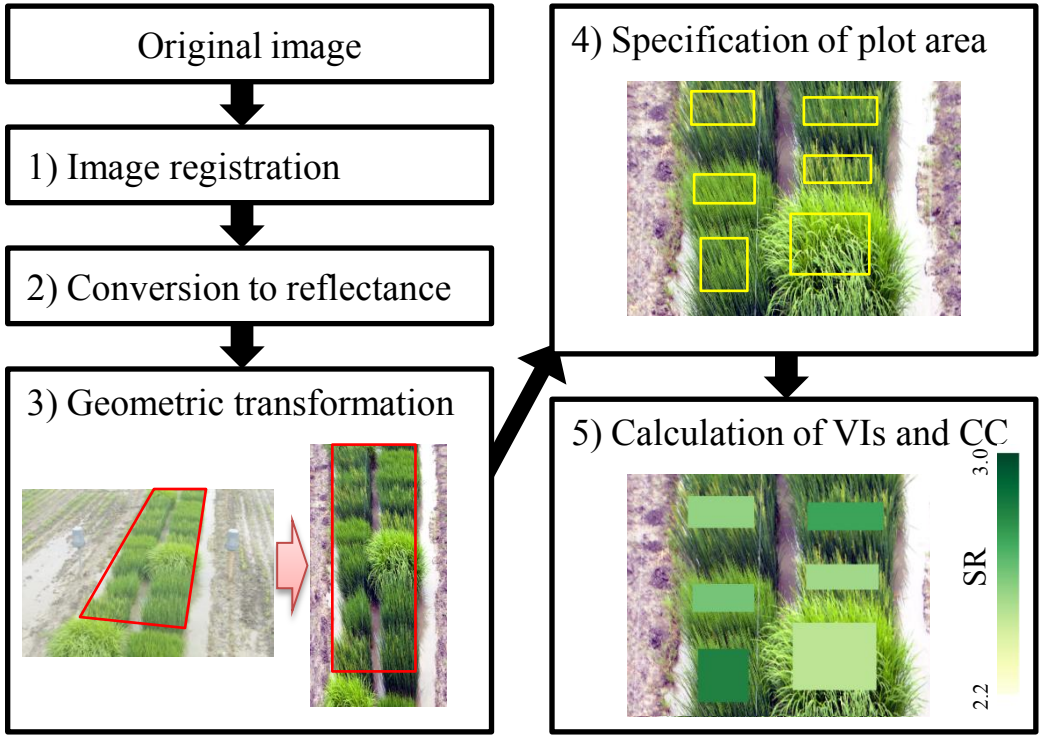
Original image
1) Image registration
2) Conversion to reflectance
3) Geometric transformation
4) Specification of plot area
5) Calculation of VIs and CC
SR
3.0
2.2

Fig. 4

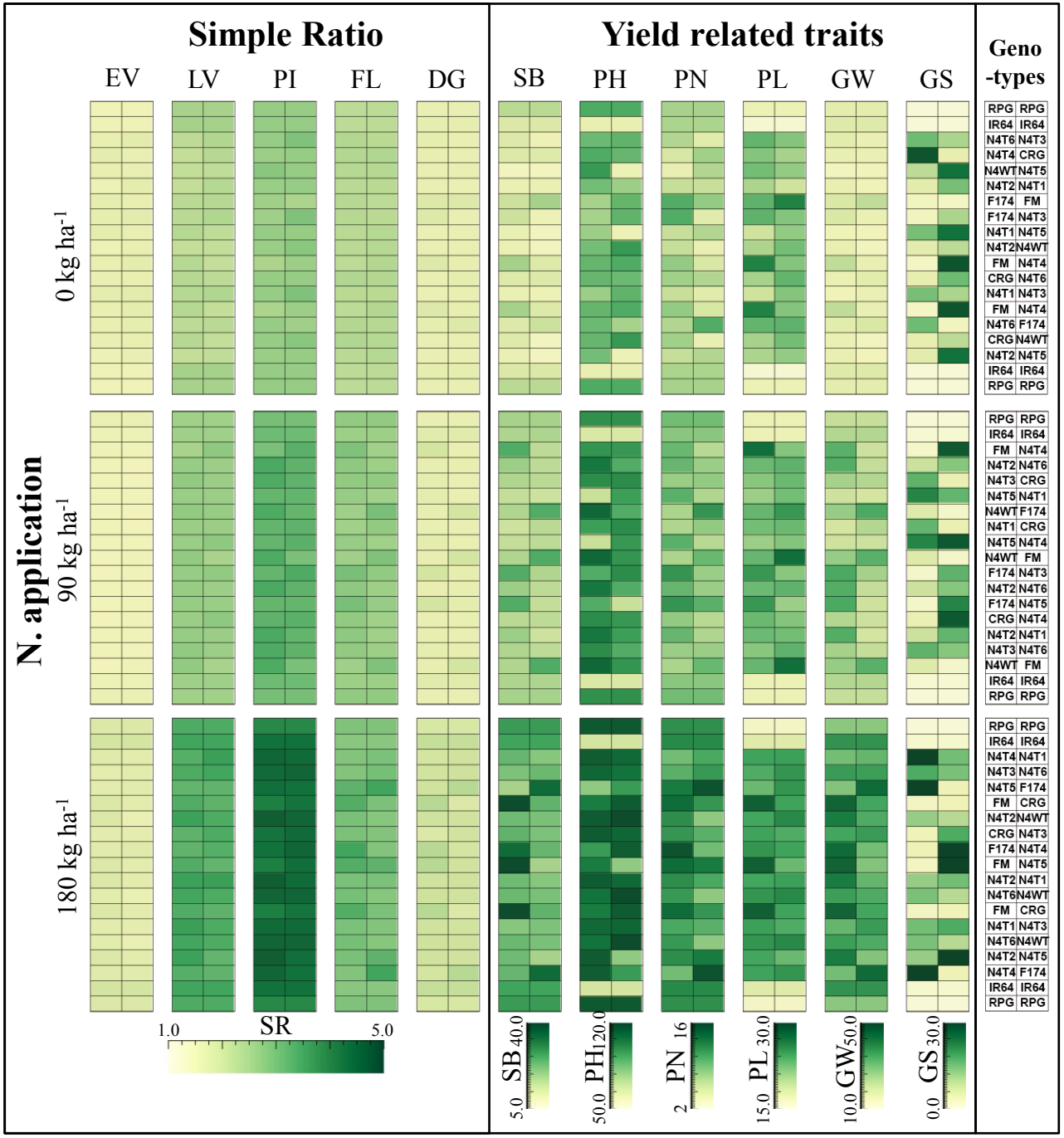
Simple Ratio
EV
LV
PI
FL
DG
Yield related traits
SB
PH
PN
PL
GW
GS
Geno -types
N. application
0 kg ha-1
90 kg ha-1
180 kg ha-1
1.0
SR
5.0
5.0 SB 40.0
50.0 PH 120.0
2 PN 16
15.0 PL 30.0
10.0 GW 50.0
0.0 GS 30.0

Fig. 5

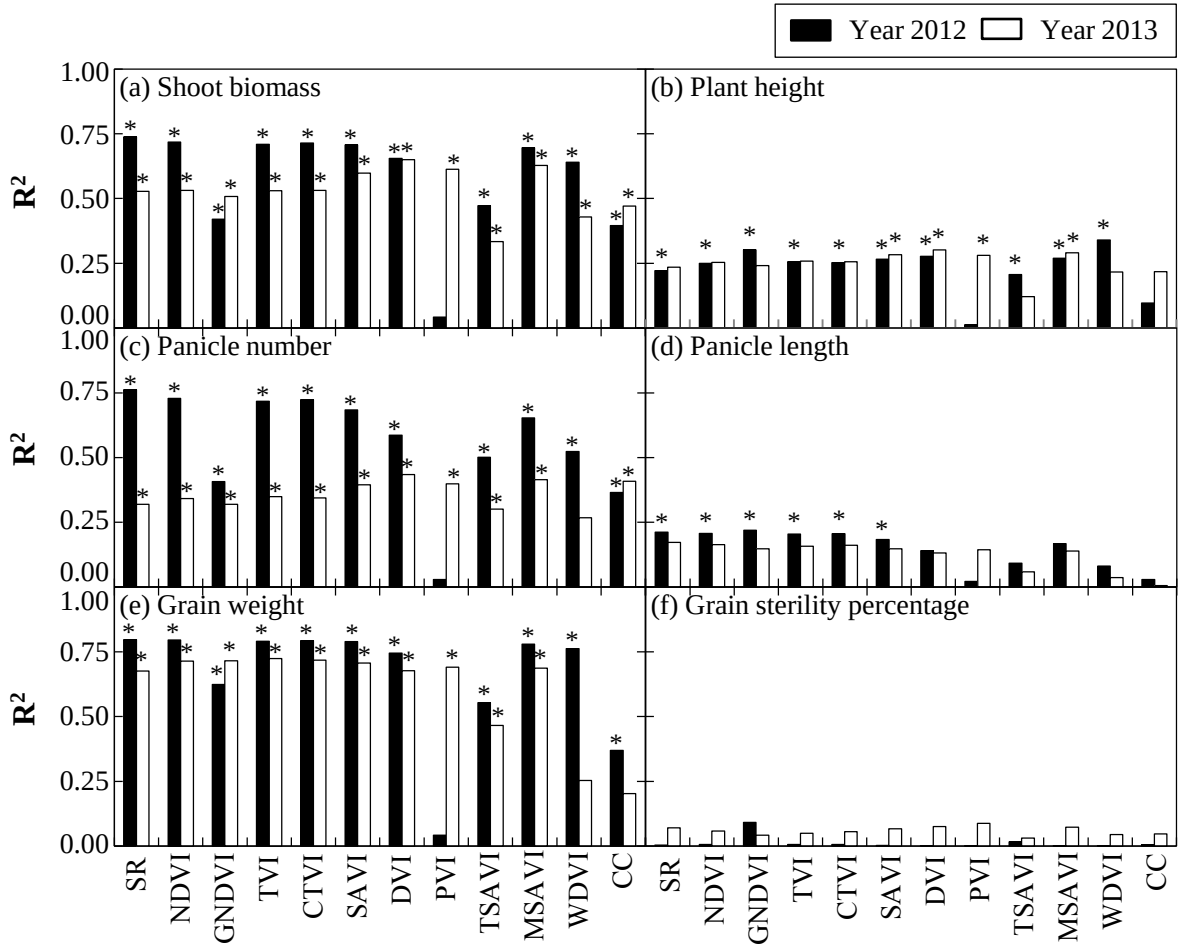

* means p<0.1

Fig. 6

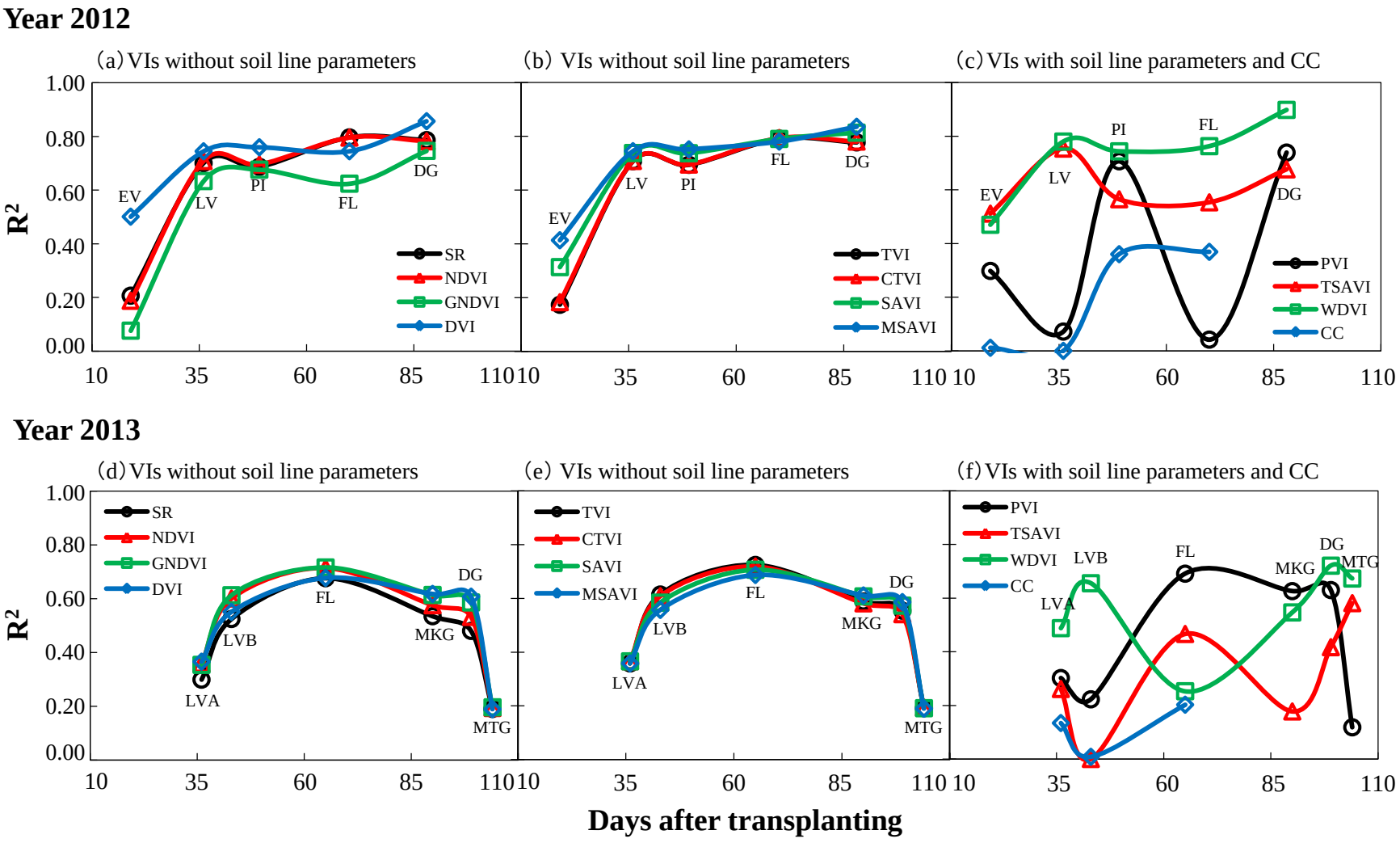
Year 2012
(a) VIs without soil line parameters
(b) VIs without soil line parameters
(c) VIs with soil line parameters and CC
Year 2013
(d) VIs without soil line parameters
(e) VIs without soil line parameters
(f) VIs with soil line parameters and CC
R²
1.00
0.80
0.60
0.40
0.20
0.00
10
35
60
85
110
EV
LV
PI
FL
DG
LVA
LVB
MKG
MTG
SR
NDVI
GNDVI
DVI
TVI
CTVI
SAVI
MSAVI
PVI
TSAVI
WDVI
CC
Days after transplanting

Fig. 7

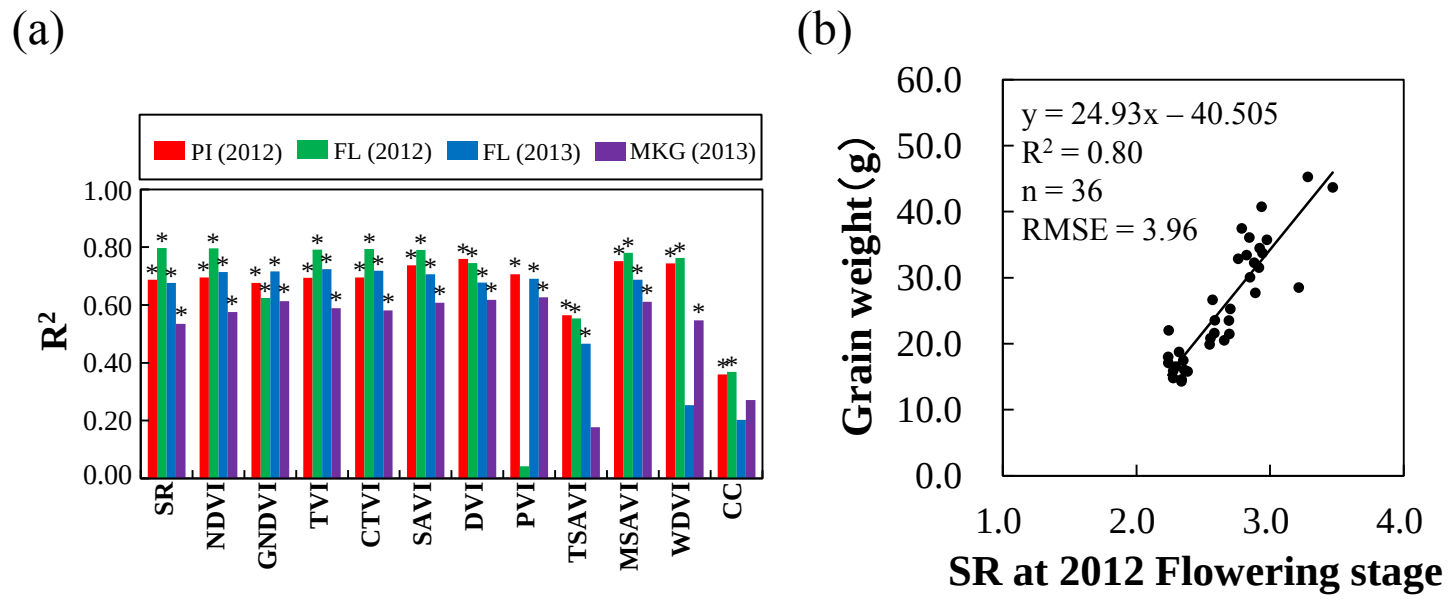
(a)
PI (2012)
FL (2012)
FL (2013)
MKG (2013)
R2
1.00
0.80
0.60
0.40
0.20
0.00
SR
NDVI
GNDVI
TVI
CTVI
SAVI
DVI
PVI
TSAVI
MSAVI
WDVI
CC
(b)
y = 24.93x – 40.505
R2 = 0.80
n = 36
RMSE = 3.96
Grain weight (g)
60.0
50.0
40.0
30.0
20.0
10.0
0.0
1.0
2.0
3.0
4.0
SR at 2012 Flowering stage

Fig. 8

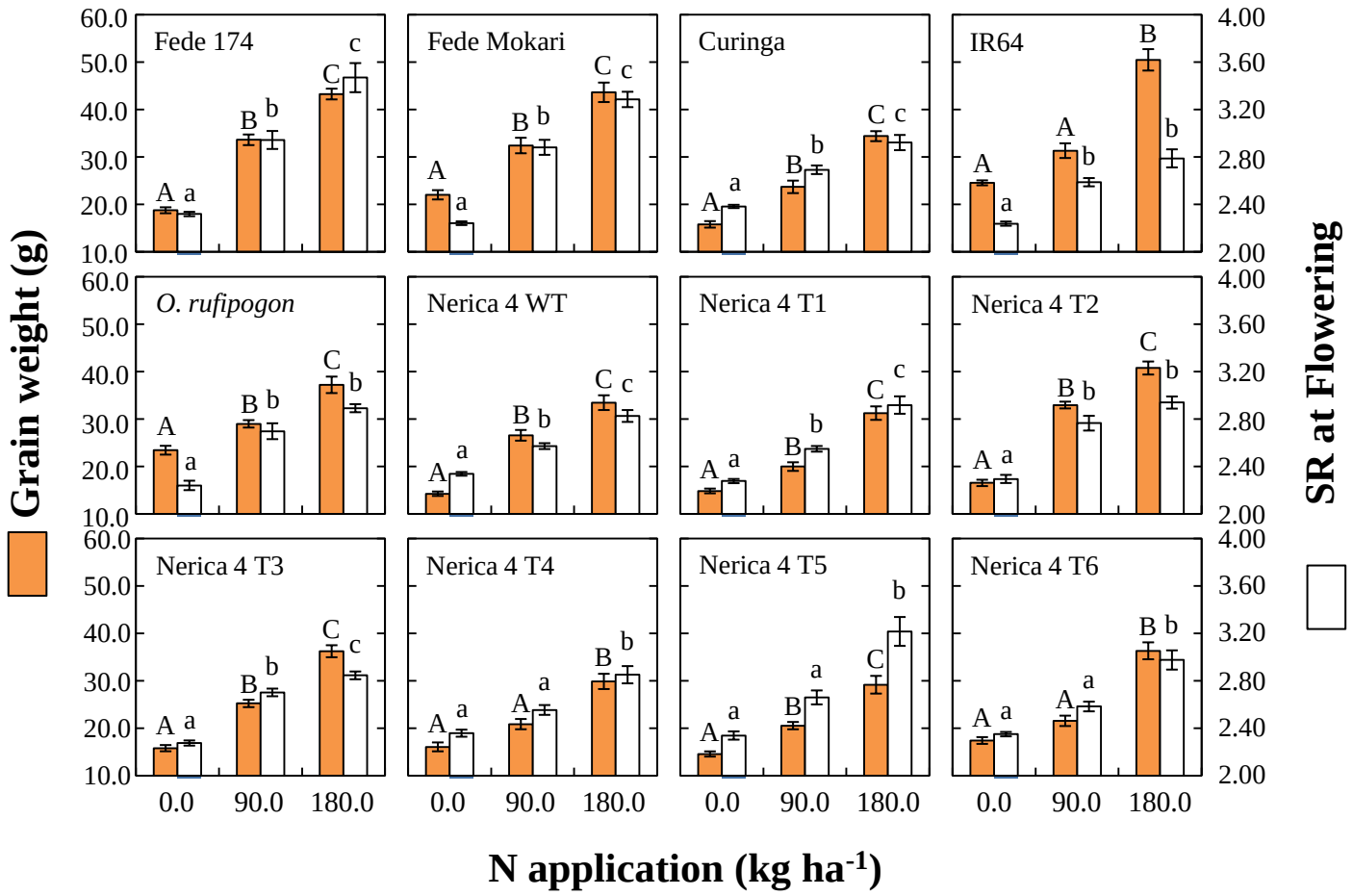
Fede 174
Fede Mokari
Curinga
IR64
O. rufipogon
Nerica 4 WT
Nerica 4 T1
Nerica 4 T2
Nerica 4 T3
Nerica 4 T4
Nerica 4 T5
Nerica 4 T6
Grain weight (g)
SR at Flowering
N application (kg ha-1)
0.0
90.0
180.0
10.0
20.0
30.0
40.0
50.0
60.0
2.00
2.40
2.80
3.20
3.60
4.00